The Journal of Chemical Physics ARTICLE scitation.org/journal/jcp

4-component relativistic Hamiltonian with effective QED potentials for molecular calculations

Cite as: J. Chem. Phys. 157, 164101 (2022); doi: 10.1063/5.0116140
Submitted: 28 July 2022 • Accepted: 14 September 2022 •
Published Online: 24 October 2022

Ayaki Sunaga,[a),b)] Maen Salman, and Trond Saue[c)]

AFFILIATIONS

Laboratoire de Chimie et Physique Quantique, UMR 5626 CNRS—Université Toulouse III-Paul Sabatier, 118 Route de Narbonne, F-31062 Toulouse, France

[a)]**Also at:** Institute for Integrated Radiation and Nuclear Science, Kyoto University, 2, Asashiro-Nishi, Kumatori-cho, Sennan-gun, Osaka 590-0494, Japan.
[b)]**Current address:** Department of Physics, Graduate School of Science, Kyoto University, Kyoto 606-8502, Japan.
[c)]**Author to whom correspondence should be addressed:** trond.saue@irsamc.ups-tlse.fr. **URL:** http://dirac.ups-tlse.fr/saue

ABSTRACT

We report the implementation of effective quantum electrodynamics (QED) potentials for all-electron four-component relativistic molecular calculations using the DIRAC code. The potentials are also available for two-component calculations, being properly picture-change transformed. The latter point is important; we demonstrate through atomic calculations that picture-change errors are sizable. Specifically, we have implemented the Uehling potential [E. A. Uehling, Phys. Rev. **48**, 55 (1935)] for vacuum polarization and two effective potentials [P. Pyykkö and L.-B. Zhao, J. Phys. B: At., Mol. Opt. Phys. **36**, 1469 (2003) and V. V. Flambaum and J. S. M. Ginges, Phys. Rev. A **72**, 052115 (2005)] for electron self-energy. We provide extensive theoretical background for these potentials, hopefully reaching an audience beyond QED specialists. We report the following sample applications: (i) We first confirm the conjecture of P. Pyykkö that QED effects are observable for the AuCN molecule by directly calculating ground-state rotational constants B_0 of the three isotopomers studied by microwave spectroscopy; QED brings the corresponding substitution Au–C bond length r_s from 0.23 to 0.04 pm agreement with experiment. (ii) In regard to spectroscopic constants of van der Waals dimers M_2 (M = Hg, Rn, Cn, Og), QED induces bond length expansions on the order of 0.15(0.30) pm for row 6(7) dimers. (iii) We confirm that there is a significant change of valence s population of Pb in the reaction $PbH_4 \rightarrow PbH_2 + H_2$, which is thereby a good candidate for observing QED effects in chemical reactions, as proposed in [K. G. Dyall *et al.*, Chem. Phys. Lett. **348**, 497 (2001)]. We also find that whereas in PbH_4 the valence $6s_{1/2}$ population resides in bonding orbitals, it is mainly found in nonbonding orbitals in PbH_2. QED contributes 0.32 kcal/mol to the reaction energy, thereby reducing its magnitude by −1.27%. For corresponding hydrides of superheavy flerovium, the electronic structures are quite similar. Interestingly, the QED contribution to the reaction energy is of quite similar magnitude (0.35 kcal/mol), whereas the relative change is significantly smaller (−0.50%). This curious observation can be explained by the faster increase in negative vacuum polarization over positive electron self-energy contributions as a function of nuclear charge.

I. INTRODUCTION

Relativistic quantum chemistry is the proper framework for the theoretical study of heavy elements.[1–5] For example, the yellow color of gold[6,7] and the cell potential of the lead-acid battery[8] cannot be explained without relativistic effects. Even for light elements, the fine structure of their spectra is essentially due to spin–orbit (SO) interaction (e.g., Refs. 9–11).

Improvements in both computational power and methodology nowadays allow highly accurate electronic structure calculations including both relativistic and electron correlation effects. A next challenge for increased accuracy is the inclusion of the effects of quantum electrodynamics (QED), which in principle means going beyond the no-pair approximation.[5,12,13] We focus on QED effects generating the Lamb shift, roughly described as follows:

- Vacuum polarization (VP): A charge in space is surrounded by virtual electron–positron pairs and this contributes to its observed charge.
- The electron self-energy (SE): The electron drags along its electromagnetic field and this contributes to its observed mass.

For hydrogen, the splitting between the $^2S_{1/2}$ and $^2P_{1/2}$ states is a mere 4 meV,[14] but for U^{91+}, it has grown to a whopping 468 eV.[15] QED effects would possibly constitute the final correction to chemistry concerning the fundamental interparticle interactions because the next contribution, parity nonconservation (PNC) associated with the weak force, is typically ten orders of magnitude smaller.[16] The magnitude of QED effects has been estimated based on the ionization potential (IP) of alkali atoms, and the *rule of thumb* is that QED effects reduce relativistic effects by about 1%.[17]

Calculations within the rigorous QED framework have been reported for few-electron systems, and they are in excellent agreement with experiment. Examples are the Lamb shift of Li-like uranium,[18,19] the hyperfine coupling constant (HFCC) of few-electron atoms,[20,21] and the anomalous g factor,[22] thus, providing stringent tests of the accuracy of QED.

The rigorous QED approach for few-electron systems cannot be extended to many-electron systems because of the high computational cost involved. A more practical, but approximate, approach is the introduction of effective QED potentials (effQED).[23–27] In the atomic case, some codes for the calculation with effective potentials have been reported (e.g., GRASP,[28] QEDMOD,[29,30] and AMBiT[31]). A nice illustration is the recent work by Pašteka *et al.*,[32] which was finally able to bring the calculated ionization potential (IP) and the electron affinity (EA) of the gold atom into meV agreement with experiment, with the high-order electron correlation being the missing crucial ingredient.

For the case of molecules in chemistry, pioneering works have been done by Kirk Peterson's group. They added the following parameterized model potentials to the all-electron scalar Douglas–Kroll–Hess (DKH) Hamiltonian:[33–37] (i) an effective SE potential in the form of a single Gaussian function, proposed by Pyykkö and Zhao (PZ)[24] and (ii) five Gaussian functions fitted by Peterson's group[33–35] to a parameterized expression for the Uehling VP potential[23] given in Ref. 17 and corrected in Ref. 24. They then found that the QED effects on the dissociation energy are about 0.6 and 0.4 kcal/mol in closed- and open-shell Hg systems, respectively.[33] A bond length expansion of 0.001 Å was observed for the HgBr molecule.[34] Dolg and co-workers have reported pseudopotentials (PPs) fitted to include QED effects.[38–40] For Cn_2, a bond length expansion due to QED of about 0.003 Å was reported,[40] in line with the effect observed by Peterson's group.[34] On the other hand, in Ref. 41, the QED effect was found to *shorten* the bond length of TsH^+, LvH, and OgH^+. The reason for this opposite trend may be that the valence orbitals have p-orbital, rather than s-orbital, contributions from the heavy atom.

PPs are widely used for the inclusion of relativistic effects, and they generally give accurate results for valence properties compared with all-electron calculations.[42,43] However, the PP approach cannot be applied to molecular core-properties, such as nuclear magnetic resonance (NMR) and Mössbauer parameters, which bars the possibility to investigate the effect of QED in the nuclear region where such effects are generated.[44] The effQED approach promoted by the Peterson group can in principle be applied to core-properties, but it should be noted that effQED potentials were added to approximate one-component relativistic Hamiltonians without picture-change.[45–47] To include QED effects in a more rigorous manner, it seems more appropriate to include effective QED potentials in four-component relativistic all-electron calculations.

In this work, we report the implementation of effective QED potentials in the DIRAC code for relativistic molecular calculations.[48] Three potentials have been implemented: the Uehling potential[23] for vacuum polarization, Pyykkö and Zhao's model SE potential,[24] and the effective SE potential of Flambaum and Ginges (FG).[25] Our implementation is based on numerical routines from the GRASP atomic code[28] that have been grafted onto the DFT grid of DIRAC.[49]

As first molecular applications of our implementation, we have chosen three case studies:

- the AuCN molecule for which Pekka Pyykkö has suggested QED effects on the bond length;[50]
- the van der Waals dimers M_2 (M = Hg, Rn, Cn, Og) for which one might suspect QED effects to be on par with interaction energies—interestingly, van der Waals forces have been described in terms of vacuum fluctuations;[51,52] and
- the reaction energy of Pb hydrides, $PbH_4 \rightarrow PbH_2 + H_2$, suggested by Dyall *et al.* as a possible candidate for a significant QED effect in chemistry.[53] In addition to the Pb system, we have also calculated the heavier analog, Fl hydrides.

Very recently, Leonid Skripnikov reported the implementation of effective QED potentials for four-component all-electron molecular calculations, so far with a focus on transition energies.[54] The initial report has been followed by applications to Ba^+, BaF, RaF, and E120F[55] as well as the five low-lying excited states of RaF.[56] The implementation is to some extent complementary to ours in that it uses the effective SE potential proposed by Shabaev and co-workers.[26,27,29] Interestingly, the implementation is based on the DIRAC code as well.

The paper is organized as follows: In Sec. II, we review the effective QED potentials that we have implemented. In Sec. III, we discuss the numerical integration of these potentials. This is followed by Sec. IV, which gives the computational details of our calculations. Our results are presented in Sec. V, followed by conclusions in Sec. VI. We also provide an appendix with more extensive theory and reading suggestions. SI units are used throughout this paper.

II. THEORY

The starting point for our work is an electronic Hamiltonian of the generic form

$$H = V_{\mathrm{NN}} + \sum_i H_D(\boldsymbol{x}_i) + \frac{1}{2}\sum_{i\neq j} g(\boldsymbol{x}_i, \boldsymbol{x}_j), \tag{1}$$

where V_{NN} is the classical repulsion of fixed nuclei. The one-electron part is the Dirac Hamiltonian

$$H_D(\boldsymbol{x}_i) = (\beta - \mathbb{1}_4)m_e c^2 - i\hbar c\boldsymbol{\alpha}\cdot\nabla_i - e\varphi_N(\boldsymbol{x}_i), \tag{2}$$

in the electric potential φ_N of the fixed nuclei and shifted by $-m_e c^2$ to align energies with the nonrelativistic scale. In the present work, the two-electron interaction g will be the instantaneous Coulomb term supplemented with the Gaunt term.[57] Further discussion of the resulting Dirac–Coulomb–Gaunt (DCG) Hamiltonian is for instance found in Ref. 3.

Our goal is to introduce QED effects, notably electron self-energy (SE) and vacuum polarization (VP), by extending the one-electron Hamiltonian by the corresponding effective QED potentials, i.e.,

$$H_D \to H_D - e\varphi_{\text{effQED}};$$
$$\varphi_{\text{effQED}} = \sum_A \left(\varphi_A^{\text{SE}} + \varphi_A^{\text{VP}}\right). \tag{3}$$

Note that the effective QED potentials are formulated as a sum over atomic contributions due to their expected short-range nature (on the order of a reduced Compton wavelength $\lambda\!\!\!^{-} = \hbar/m_e c$).[44]

In the following, we shall present the effective QED potentials selected for our implementation with some remarks on their construction, which may provide indications on their expected performance. We shall proceed within the $\hat{\mathcal{S}}$-matrix (scattering matrix) formalism of QED. Since we hope to address a wider audience than QED specialists, we provide a more extensive theoretical background in the Appendix.

QED is the relativistic quantum field theory that describes the interaction of electromagnetic radiation with relativistic matter (Dirac electrons). The interaction between electrons and photons is given by an interaction-Hamiltonian density

$$\hat{\mathcal{H}}_I(x) = -ec\bar{\hat{\Psi}}(x)\gamma^\mu\hat{\Psi}(x)\hat{A}_\mu(x). \tag{4}$$

Here, $\hat{\Psi}(x)$ and $\bar{\hat{\Psi}}(x)$ are the quantized Dirac field operator and its corresponding adjoint, respectively, whereas $\hat{A}_\mu(x)$ is the quantized photon field operator. The job of these operators is to create and annihilate, at the spacetime point $x = (ct, \boldsymbol{x})$, electrons and photons, respectively. This last expression accounts (explicitly) for the coupling between electron and photon fields, and it is obtained through minimal substitution of the four-gradient of the Dirac Lagrangian density in accordance with the *principle of minimal electromagnetic interaction* (term coined by Gell-Mann[58]). For detailed derivations and discussions, the reader may consult Schweber in Ref. 59 (Chap. 10), Peskin and Schroeder in Ref. 60 (Chap. 4), as well as Greiner and Reinhardt in Ref. 61 (Sec. 8.6). The scattering matrix is a special case of the time-evolution operator $\hat{U}(t, t_0)$, where the initial t_0 and final times t are at $\mp\infty$, to ensure Lorentz invariance. Upon expansion of the $\hat{\mathcal{S}}$-matrix operator in the fundamental charge e, the nth-order term $\hat{\mathcal{S}}^{(n)}$ contains a time-ordered string of n interaction-Hamiltonian densities $\mathcal{H}_I$, as seen in Eq. (A29). Using Wick's theorem,[62] a time-ordered string is converted into a linear combination of normal-ordered ones with all possible contractions, which in turn can be translated into the iconic Feynman diagrams.[63] We limit attention to systems of n electrons and zero photons (photon vacuum). The latter implies that any string of normal-ordered photon operators $\hat{A}_\mu(x)$ that is not fully contracted will vanish upon taking expectation values, such that the $\hat{\mathcal{S}}$-matrix expansion is effectively limited to even-ordered contributions, associated with the fine-structure constant $\alpha = e^2/4\pi\varepsilon_0\hbar c$ as expansion parameter. To lowest order in α appears five Feynman diagrams, shown in Fig. 1: Two of them give state-independent energy-shifts and are usually ignored within a perturbative setting, whereas the remaining three represent electron self-energy, vacuum polarization, and single-photon exchange. The latter diagram describes the relativistic electron–electron interaction, mediated by photons, to lowest order and is in line with the statement of Dirac:

> Classical electrodynamics, in its accurate (restricted) relativistic form, teaches us that the idea of an interaction energy between particles is only an approximation and should be replaced by the idea of each particle emitting waves, which travel outward with a finite velocity and influence the other particles in passing over them.[64]

In the diagrams of Fig. 1, double electron lines appear to indicate that we are working within the Bound-State QED (BSQED) framework in which the Dirac field operators are expanded in solutions of the Dirac equation in some external (contravariant) four-potential, i.e., $A^e = (\varphi^e/c, \boldsymbol{A}^e)$ (Furry picture[65]), rather than free-particle ones. In the atomic case, this provides us with a second perturbation expansion parameter $Z\alpha$, as will be seen in Sec. II A.

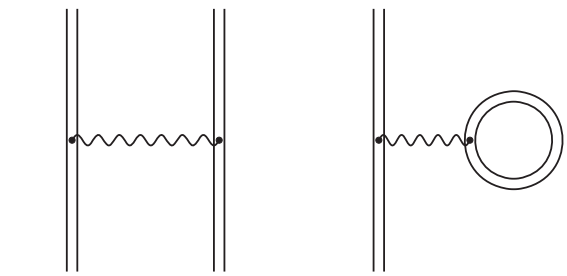

(a) Single-photon exchange. (b) Vacuum polarization.

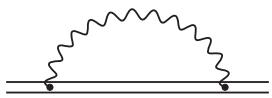

(c) Self-energy.

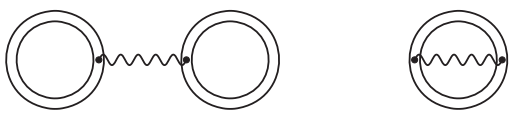

(d) Direct bubble diagram. (e) Exchange bubble diagram.

FIG. 1. The lowest-order QED corrections for a many-bound-electron system of order α. (a)-(e).

A. Effective QED potentials for vacuum polarization

The four-potential associated with the vacuum polarization effect can be written as

$$\varphi^{\mu}_{\rm VP}(\boldsymbol{x}_1) = \frac{e}{2\pi i}\int_{C_F} dz \int d^3x_2 \frac{{\rm Tr}\left[\gamma^{\mu} G_{A^e}(\boldsymbol{x}_2,\boldsymbol{x}_2;z)\gamma^0\right]}{4\pi\epsilon_0|\boldsymbol{x}_1-\boldsymbol{x}_2|}, \tag{5}$$

where the complex z-integral is to be evaluated along the Feynman contour C_F that goes above and below positive- and negative-energy poles, respectively, of the bound-electron Green's function G_{A^e}. This function is related to the bound-electron propagator $S^F_{A^e}$ by Eq. (A42). This VP potential leads to the following vacuum polarization energy-shifts:

$$\Delta E^{\alpha,2}_{\rm VP} = -e\sum_i \int d^3x \bar{\psi}_i(\boldsymbol{x})\gamma_{\mu}\psi_i(\boldsymbol{x})\varphi^{\mu}_{\rm VP}(\boldsymbol{x}). \tag{6}$$

From consideration of time-reversal symmetry, one can show that in the case of a purely scalar external potential given by $A^e = (\varphi^e/c, \boldsymbol{0})$, the vector components of the vacuum polarization four-potential vanish,

$$\varphi^{\mu}_{\rm VP}(\boldsymbol{x}) = 0 \qquad \text{for} \quad \mu = 1,2,3. \tag{7}$$

The bound Green's function G_{A^e} can be written in terms of the free Green's function G_0 and expanded in powers of the time-independent external potential A^e (hence, $Z\alpha$ in the atomic case) as shown in Eq. (A44). As discussed in Subsection 6 b of the Appendix, the first nonvanishing term of this expansion is the one that is linear in the external potential $A^e(\boldsymbol{x})$ (the one-potential term). The potential of Eq. (5) is divergent (as seen in Subsection 6 b of the Appendix) and calls for regularization and renormalization (see Subsection 6 d of the Appendix). After employing these techniques, one can extract the physical contribution associated with this vacuum polarization effect and, in the point nucleus problem, represent it by the following scalar potential:[23]

$$\varphi^{\rm point}_{\rm Ueh.}(\boldsymbol{x}) = \frac{Ze}{4\pi\epsilon_0 r_x}\frac{2\alpha}{3\pi}K_1\left(\frac{2r_x}{\lambda\!\!\!^{-}}\right), \tag{8}$$

which corrects the classical Coulomb potential. Here, $r_x \equiv |\boldsymbol{x}|$ is the radial distance and is expressed in terms of the function[66]

$$K_1(x) = \int_1^{\infty} d\zeta e^{-x\zeta}\left(\frac{1}{\zeta^2}+\frac{1}{2\zeta^4}\right)\sqrt{\zeta^2-1} \tag{9}$$

(see also Refs. 67 and 68). This potential is named after Uehling, who first calculated it in 1935 for a point charge nuclear distribution (as indicated by the superscript "point"). The corresponding potential for an arbitrary nuclear distribution $\rho^{\rm nuc.}$, normalized to one, is obtained by the following convolution:[66]

$$\varphi^{\rm nuc.}_{\rm Ueh.}(\boldsymbol{x}) = \int d^3y\, \rho^{\rm nuc.}(\boldsymbol{y})\varphi^{\rm point}_{\rm Ueh.}(\boldsymbol{x}-\boldsymbol{y}). \tag{10}$$

In the case of a spherically symmetric nuclear charge distribution, one obtains, after angular integration,[66]

$$\varphi^{\rm nuc.}_{\rm Ueh.}(\boldsymbol{x}) = \frac{Ze}{4\pi\epsilon_0 r_x}\lambda\!\!\!^{-}\frac{2\alpha}{3}\int_0^{\infty} r_y dr_y \rho^{\rm nuc.}(r_y) \times\left[K_0\left(\frac{2}{\lambda\!\!\!^{-}}|r_x-r_y|\right)-K_0\left(\frac{2}{\lambda\!\!\!^{-}}|r_x+r_y|\right)\right], \tag{11}$$

where appears the function

$$K_0(x) = \int_1^{\infty} d\zeta e^{-x\zeta}\left(\frac{1}{\zeta^3}+\frac{1}{2\zeta^5}\right)\sqrt{\zeta^2-1}. \tag{12}$$

The integral functions K_0 and K_1 are related through

$$K_1(x) = -\frac{d}{dx}K_0(x). \tag{13}$$

The Uehling potential generally represents the dominant vacuum polarization effect.[19,69] The Feynman diagram associated with this process is presented in Fig. 3(b) and is associated with the $\alpha(Z\alpha)$ perturbation order. The higher-order vacuum polarization potentials, associated with the Wichmann–Kroll,[70] $\alpha(Z\alpha)^3$, and Källén–Sabry,[71] $\alpha^2(Z\alpha)$, processes, are briefly discussed at the end of Subsection 6 b of the Appendix.

B. Effective QED potentials for self-energy

The energy-shift associated with the self-energy process, in which an electron emits and absorbs a virtual-photon, is given by the following expression:

$$\Delta E^{\alpha,2}_{\rm SE} = -e\sum_i \int d^3x_1 \int d^3x_2 \psi^{\dagger}_i(\boldsymbol{x}_2)\varphi_{\rm SE}(\boldsymbol{x}_2,\boldsymbol{x}_1;E_i)\psi_i(\boldsymbol{x}_1). \tag{14}$$

This expression probably originated from the work of Baranger *et al.*[72] (Sec. II). Notice at this point that unlike the vacuum polarization effect that is represented by a local scalar potential, the self-energy effect is represented by a nonlocal matrix potential given by

$$\varphi_{\rm SE}(\boldsymbol{x}_2,\boldsymbol{x}_1;E_i) = -\frac{e}{2\pi i}\int_{C_F} dz \alpha^{\mu} G_{A^e}(\boldsymbol{x}_2,\boldsymbol{x}_1;z)\alpha_{\mu} \times\frac{\exp(g(\boldsymbol{x}_2,\boldsymbol{x}_1;z-E_i))}{4\pi\epsilon_0|\boldsymbol{x}_1-\boldsymbol{x}_2|}, \tag{15}$$
$$g(\boldsymbol{x}_2,\boldsymbol{x}_1;z) = +\frac{i}{\hbar}|\boldsymbol{x}_1-\boldsymbol{x}_2|\sqrt{z^2/c^2+i\epsilon}.$$

Here, ϵ is a small positive number, and the z-integral is again to be evaluated along the Feynman contour C_F. This expression is obtained using the covariant Feynman gauge photon propagator. The corresponding expression obtained using Coulomb gauge photon propagator is given by Lindgren in Ref. 73 (Sec. 4.6.1.2) (see also Malenfant in Ref. 74). As in the vacuum polarization case, the self-energy potential of Eq. (15) is divergent (as seen in Subsection 6 c of the Appendix) and calls for a regularization and renormalization treatment in order to extract the physical (finite) correction; see Subsection 6 d of the Appendix.

In the next two sections, we shall assume that the nonlocal potential of Eq. (15) can be written in terms of a local effective potential $\varphi_{\rm SE}(\boldsymbol{x}_1)$ as

$$\varphi_{\rm SE}(\boldsymbol{x}_2,\boldsymbol{x}_1;E_i) \approx \varphi_{\rm SE}(\boldsymbol{x}_1)\delta(\boldsymbol{x}_2-\boldsymbol{x}_1), \tag{16}$$

and we discuss some choices of $\varphi_{\rm SE}(\boldsymbol{x}_1)$ that are designed to reproduce some precise self-energy correction calculations and are employed in our numerical calculations.

1. Pyykkö and Zhao SE potential

In Ref. 24, Pyykkö and Zhao (PZ) proposed a simple local self-energy potential of the following form:

$$\varphi_{\rm SE}(\boldsymbol{x}) = Be^{-\beta r_x^2}. \tag{17}$$

The parameters B and β are quadratic nuclear charge (Z) dependent functions given by

$$B(Z) = -48.6116 + 1.536\,66\,Z + 0.030\,112\,9\,Z^2, \tag{18}$$

$$\beta(Z) = -12\,751.3 + 916.038\,Z + 5.7797\,Z^2, \tag{19}$$

where the six decimal numbers were chosen to fit precise $29 \le Z \le 83$ atomic calculations of the renormalized self-energy correction in all orders of $(Z\alpha)^{n\ge0}$ to the

1. 2s energy-levels of the hydrogen-like systems, i.e., the renormalized version of Eq. (14), taken from calculations of (1) Beier *et al.*[69] with nuclear charges $26 \le Z \le 110$, using a homogeneously charged sphere nuclear model, and (2) Indelicato and Mohr[75] with Coulombic nuclear charges of $5 \le Z \le 90$ and
2. M1 hyperfine splitting for lithium-like atoms taken from calculations[76] of Boucard and Indelicato[77] done on stable isotopes with $3 \le Z \le 92$.

2. Flambaum and Ginges SE potential

The starting point for the potential proposed by Flambaum and Ginges (FG)[25] is associated with the one-potential bound-state self-energy process, of order $\alpha(Z\alpha)$, given in Eqs. (A64) and (A68) and represented by Fig. 4(b). However, further modeling, including parametrization, is introduced such that the potential can account for the full self-energy process to all orders in $(Z\alpha)$ and be used in atomic calculations.

In the evaluation of matrix elements over the operator of Eq. (A68), Flambaum and Ginges employ free-particle solutions rather than atomic bound orbitals. This replacement yields the free-electron vertex-correction (VC) problem. This terminology can be understood from consideration of the scattering of a free electron due to the interaction with a classical external potential (the vertex process). In terms of momentum-space quantities [cf. Eq. (A65)], including *free*-electron field operators, the corresponding (non-radiative) $\mathcal{S}$-matrix is given by

$$\hat{\mathcal{S}}^{(1)}_{\rm scattering} = -\frac{e}{i\hbar}\int\frac{d^4p_2}{(2\pi\hbar)^4}\int\frac{d^4p_1}{(2\pi\hbar)^4} :\bar{\hat{\Psi}}(p_2)\gamma^\mu A^e_\mu(p_2-p_1)\hat{\Psi}(p_1): \tag{20}$$

(see for instance Sec. 8.7 in Ref. 78). This process is represented in the left panel of Fig. 2, where the wiggly line ending with a cross × describes an interaction of a free electron with the classical external potential source through the exchange of a four-momentum $q = p_2 - p_1$. We note that in general a factor $(-e\gamma^\mu)$ is associated with each space-time point (vertex). The right panel of Fig. 2 represents

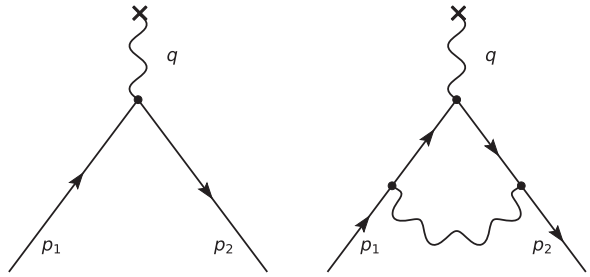

(a) Classical scattering process. (b) First radiative correction.

FIG. 2. Momentum-space Feynman diagrams for the lowest-order scattering processes through (the exchange of) momentum-transfer $q = p_2 - p_1$. (a) and (b).

one of the four lowest-order radiative corrections to the left panel process. The corresponding $\mathcal{S}$-matrix can be combined with the one of Eq. (20) through the substitution

$$\gamma^\mu \to \Gamma^\mu = \gamma^\mu + \Lambda^\mu(p_2,p_1), \tag{21}$$

where the vertex-correction function $\Lambda^\mu(p_2,p_1)$ is given by Eq. (A69). After a careful treatment of the divergence when $q = 0$, as done in Refs. 60 (Sec. 6.3) and 79 (Sec. 117), one obtains the regularized (physical) vertex-correction function $\Lambda^\mu_R(p_2,p_1)$. Furthermore, using the fact that the vertex function is sandwiched between free-electron (on-mass-shell) field operators, one can show that this function can be written as

$$\Lambda^\mu_R(q) = \gamma^\mu F_1(q^2) + \frac{i}{2m_ec}\sigma^{\mu\nu}q_\nu F_2(q^2), \tag{22}$$

where $\sigma^{\mu\nu} = \frac{i}{2}[\gamma^\mu,\gamma^\nu]$, and F_1 and F_2 are known as the electric and magnetic form factors, respectively [corresponding to $f-1$ and g in Eq. (116.6) of Ref. 79]. The term "form factor" comes from diffraction physics; see for instance Ref. 80.

Since the free-electron vertex function of Eq. (22) only depends on the momentum-transfer $q = p_2 - p_1$, it conveniently yields a local potential in real space. This can be clearly seen from the following relation:

$$\int\frac{d^4p_2}{(2\pi\hbar)^4}\int\frac{d^4p_1}{(2\pi\hbar)^4}\bar{\hat{\Psi}}(p_2)\Lambda^\mu_R(q)A^e_\mu(q)\hat{\Psi}(p_1) = \frac{1}{c}\int d^4x\hat{\Psi}^\dagger(x)\varphi_{\rm VC}(x)\hat{\Psi}(x). \tag{23}$$

When the nucleus is described as a point charge, the corresponding Coulomb potential,

$$A^e_0(q) = \delta(q_0)\frac{2\pi\hbar^3}{c\epsilon_0}\frac{Ze}{\boldsymbol{q}^2}, \tag{24}$$

generates a vertex-correction potential of the form

$$\varphi^{\rm point}_{\rm VC}(\boldsymbol{x}) = \frac{\hbar^2}{\epsilon_0}\int\frac{d^3q}{(2\pi\hbar)^3}e^{+\frac{i}{\hbar}\boldsymbol{q}\cdot\boldsymbol{x}}\frac{Ze}{\boldsymbol{q}^2}\left[F_1(-\boldsymbol{q}^2)+\frac{1}{2m_ec}\boldsymbol{\gamma}\cdot\boldsymbol{q}F_2(-\boldsymbol{q}^2)\right] = \varphi^{\rm point}_{\rm elec}(\boldsymbol{x}) + \varphi^{\rm point}_{\rm mag}(\boldsymbol{x}), \tag{25}$$

which splits into electric and magnetic scalar potentials. We note that due to the time-independence of the Coulomb potential, the time-like part of the four-momentum transfer $q = p_2 - p_1$ vanishes. In terms of the variable $t = q^2 = -\boldsymbol{q}^2$, the form factors are Hermitian analytic functions,[81] i.e.,

$$F(t) = F^*(t^*). \tag{26}$$

This feature, combined with these functions being radial in terms of $\boldsymbol{q}$ and the clever use of complex analysis techniques, allowed Berestetskii *et al.* to express such functions in coordinate-space using only their imaginary parts in momentum-space,

$$F(\boldsymbol{x}) = \frac{1}{(2\pi\hbar)^2 r_x} \int_{4m_e^2c^2}^{\infty} dt\, \Im[F(t)] \exp\left[-\frac{1}{\hbar} r_x \sqrt{t}\right] \tag{27}$$

[see Eq. (114.4) of Ref. 79]. It may be noted that the lower limit of integration over t is $4m_e^2c^2$, corresponding to the threshold of pair creation.[82] Expressions for the imaginary part of the form factors can be found in Refs. 79 [Eqs. (117.14) and (117.15)] and 83 [Eq. (2.12)],

$$\Im[F_1(t)] = \frac{\alpha}{\sqrt{t(t-4m_e^2c^2)}}\left[2m_e^2c^2 - 3t/4 + \left(t/2 - m_e^2c^2\right)\log\left(\frac{t-4m_e^2c^2}{\lambda^2}\right)\right], \tag{28}$$

$$\Im[F_2(t)] = \frac{\alpha m^2c^2}{\sqrt{t(t-4m_e^2c^2)}}. \tag{29}$$

Building on the work of Berestetskii *et al.*,[79] Flambaum and Ginges have evaluated the integral of Eq. (25) and obtained the associated real-space potentials. After the variable substitution $t = 4m_e^2c^2\zeta^2$, the magnetic potential was found to be

$$\varphi_{\mathrm{mag}}^{\mathrm{point}}(\boldsymbol{x}) = \frac{\alpha\hbar}{4\pi m_e c} i\boldsymbol{\gamma}\cdot\nabla_x\left[\frac{Ze}{4\pi\varepsilon_0 r_x}\left(K_m\left(\frac{2r_x}{\lambda\!\!\!^{-}}\right) - 1\right)\right], \tag{30}$$

where we have introduced the function

$$K_m(x) = \int_1^{\infty} d\zeta\, \frac{e^{-x\zeta}}{\zeta^2\sqrt{\zeta^2-1}}, \tag{31}$$

which can be recognized as the second Bickley–Naylor function Ki_2 (cf. Ref. 68). Note that the same variable ζ is employed in the Uehling potential [cf. Eqs. (9) and (12)]. The magnetic contribution gives the first-order correction to the magnetic moment: the anomalous magnetic moment of the electron, first calculated by Schwinger, see for instance Mandl and Shaw in Ref. 78 (Sec. 10.5).

On the other hand, the electric form factor yields the electric effective potential given by

$$\varphi_{\mathrm{elec}}^{\mathrm{point}}(\boldsymbol{x},\lambda) = -\frac{\alpha}{\pi}\frac{Ze}{4\pi\varepsilon_0 r_x} K_e\left(\frac{2r_x}{\lambda\!\!\!^{-}}\right), \tag{32}$$

where we have introduced the function

$$K_e(x) = \int_1^{\infty} d\zeta\, \frac{e^{-x\zeta}}{\sqrt{\zeta^2-1}}\left\{-\frac{3}{2} + \frac{1}{\zeta^2} + \left(1 - \frac{1}{2\zeta^2}\right) \times \left[\ln\left(\zeta^2-1\right) + 2\ln\left(\frac{2m_ec^2}{\lambda}\right)\right]\right\}. \tag{33}$$

These self-energy effective potentials were first derived with respect to a point nucleus (Coulomb potential), and the corresponding generalized expressions for an arbitrary normalized nuclear distribution $\rho^{\mathrm{nuc.}}$ are obtained by convolution[84] as in Eq. (10).

The potential of Eq. (32) is called the high-frequency (HF) term because it contains an energy parameter λ, already present in Eq. (28), that prevents the obtention of low-frequency (LF) contributions. This parameter is associated with the introduction of a small fictitious photon mass, which needs to be plugged in the photon propagator denominator in order to make the divergent (at small momenta) momentum-space integral—associated with the vertex-correction—convergent. Details concerning this problem are discussed by Greiner and Reinhardt in Ref. 85 [Eq. (5.91)] and Itzykson and Zuber in Ref. 86 [Eq. (7.45)], in addition to Peskin and Schroeder in Ref. 60 (pp. 195–196). We note that the remaining divergence, occurring in the limit of zero photon mass, or $\lim_{\lambda\to 0}$, is overcome by taking into account the differential cross section associated with the Bremsstrahlung effect; detailed discussions are found in Refs. 85 (pp. 311–313) and 60 (Sec. 6.4). Flambaum and Ginges choose a somewhat different strategy, which furthermore allows them to amend the fact that the used form factors are derived for the free-electron vertex-correction of order $(Z\alpha)^{n=1}$ only and now take into account complementary self-energy corrections $(Z\alpha)^n, n \neq 1$ [diagrams of Figs. 4(a), 4(c), and 4(d), and higher orders]. They write the high-frequency (HF) contribution as

$$\varphi_{\mathrm{HF}}^{\mathrm{point}}(\boldsymbol{x}) = A(Z,\boldsymbol{x})\varphi_{\mathrm{elec}}^{\mathrm{point}}(\boldsymbol{x},\lambda), \tag{34}$$

where $A(Z,\boldsymbol{x})$ is a fitting function, and choose a λ-value that will minimize the low-frequency contribution. They argue that λ should be on the order of electron binding energies, that is, $(Z\alpha)^2 m_e c^2$. They finally define it through

$$\ln\left(\frac{2m_ec^2}{\lambda}\right) = 2\ln\left(\frac{1}{Z\alpha} + \frac{1}{2}\right), \tag{35}$$

though, for better performance. Flambaum and Ginges next argue that the low-frequency (LF) potential should have the range of a 1s orbital of hydrogen-like atoms and, therefore, choose the functional form

$$\varphi_{\mathrm{LF}}^{\mathrm{point}}(\boldsymbol{x}) = -\frac{B(Z)}{e} Z^4\alpha^5 m_e c^2 e^{-Zr_x/a_0}, \tag{36}$$

where $a_0 = \lambda\!\!\!^{-}/\alpha$ is the Bohr radius and

$$B(Z) = 0.074 + 0.35 \times Z\alpha \tag{37}$$

is a second fitting function.

The fitting function of the high-frequency contribution is written as

$$A(Z,\boldsymbol{x}) = \Theta(Z,\boldsymbol{x})\left(1.071 - 1.976y^2 - 2.128y^3 + 0.169y^4\right) \tag{38}$$

in terms of the variable $y = (Z - 80)\alpha$ and a cutoff function of the form

$$\Theta(Z, \boldsymbol{x}) = \frac{r_x}{r_x + 0.07(Z\alpha)^2 \boldsymbol{\lambda}}, \tag{39}$$

which will dampen the contribution of $\varphi_{\text{elec}}^{\text{point}}$ at short distances where the locality of the effective SE potential breaks down. The coefficients of the A and B fitting functions above were adjusted to reproduce the self-energy corrections to high s- and p-states, respectively, calculated accurately in Refs. 87 and 88 for Coulombic hydrogenlike atoms of $5 \le Z \le 110$. It should be added that Thierfelder and Schwerdtfeger[89] later modified the fitting function to $A_n(Z, \boldsymbol{x})$, making it dependent on the principal quantum number n. These potentials with $A_n(Z, \boldsymbol{x})$ instead of $A(Z, \boldsymbol{x})$ were used by Pašteka *et al.* to calculate the electron affinity and ionization potential of gold.[32] Ginges and Berengut,[84] on the other hand, made both fitting functions A and B dependent on the orbital angular momentum ℓ and further suggested the introduction of a κ-dependence as well. The downside of making the effective QED potentials dependent on atomic orbital quantum numbers is that it complicates the extension of these potentials to the molecular regime. This is in fact what motivated us to implement the effective SE potentials of Pyykkö and Zhao[24] and Flambaum and Ginges[25] rather the one proposed by Shabaev and co-workers.[26,27,29]

C. Atomic shift operator

With the above effective QED potentials available in an atomic code (see Sec. III), we have investigated their extension to molecular calculations by adding to the electronic Hamiltonian, Eq. (1), an operator of the form

$$\begin{aligned} V_{\text{ASHIFT}} &= \sum_i |\psi_i\rangle \omega_i \langle \psi_i|, \\ \omega_i &= \langle \psi_i| - e\varphi_{\text{effQED}} |\psi_i\rangle, \end{aligned} \tag{40}$$

where $\{\omega_i\}$ are expectation values of the effective QED potentials taken from atomic calculations and $\{\psi_i\}$ are precalculated atomic orbitals, in practice limited to those that are occupied in the electronic ground state of the atoms constituting the molecule under study, calculated in their proper basis. The import of atomic orbitals into molecular calculations is straightforward in the case of the DIRAC code since such functionality is already available through projection analysis.[90,91] There is some overlap between the spectral representation of the self-energy proposed by Dyall[92] as well as the effective SE operator proposed by Shabaev *et al.*,[26] but those approaches are based on hydrogenic orbitals.

III. IMPLEMENTATION

Routines for the radiative potentials used in this work are available in the GRASP atomic code.[28] Routines for calculating the Uehling potential were reported as early as 1980.[93] McKenzie *et al.* follow the approach suggested by Fullerton and Rinker.[66] More precisely, they employ Eq. (11) for the inner grid points until a more approximate form, Eq. (6) of Ref. 66, becomes numerically valid. The latter form is then used until the magnitude of the potential falls below a threshold value. The effective SE potential of Flambaum and Ginges[25] was implemented more recently[89] as is also the case[94] of the effective SE potential of Pyykkö and Zhao.[24] As already mentioned, the FG potential is in principle that associated with a point nucleus, although fitting parameters have been optimized also to calculations with finite nuclear charge distributions. Thierfelder and Schwerdtfeger[89] adapted these potentials to finite nuclei by replacing the Coulomb potentials of Eqs. (30) and (32) by the potentials of finite nuclear charge distributions, and we have so far followed this approach which appears to be a reasonable approximation, as can be inferred from Table IV of Ref. 84.

We have adapted the GRASP effective QED potential routines to molecular calculations by using the numerical integration scheme implemented for relativistic Kohn–Sham calculations in the DIRAC molecular code.[49] The scheme is based on the Becke partitioning[95] of the molecular volume into atomic ones for which numerical integration is carried out in spherical coordinates. Specifically, we use Lebedev angular quadrature,[96] by default setting $\ell = 15$, combined with the basis set adaptive radial grid proposed by Lindh *et al.*[97] It may be noted that the effective QED potentials presented in Sec. II are all radial, with the exception of the magnetic contribution to the Flambaum–Ginges SE potential, Eq. (30).

Due to the very local nature of the effective QED potentials,[44] one-electron integrals over a potential associated with atomic center A can be well approximated by

$$V_{\mu\nu}^A \approx \int_0^{R_A} dr_A \int_\Omega d\Omega_A \left[\chi_\mu v^A \chi_\nu\right](\mathbf{r}_A) r_A^2, \tag{41}$$

where $\{\chi_\mu\}$ are Gaussian-type basis functions. The most delocal potential is the low-frequency contribution to the electric form factor of the Flambaum–Ginges SE potential, Eq. (36), since it has been designed to have the range of the 1s orbital of a hydrogenlike atom. For low Z, the potential may thereby overlap significantly with neighbor centers. By default, we therefore deactivate the effective QED potentials for $Z < 19$. We also determine the value of the upper limit of radial integration R_A based on the convergence of the low-frequency term to a very conservative 10^{-50}.

IV. COMPUTATIONAL DETAILS

For all calculations, we used a development version of the DIRAC code;[48,98] precise version and build information is found in the output files, see Ref. 99. A Gaussian model[100] for the nuclear charge distribution was employed throughout our calculations. Unless otherwise stated, we applied the Uehling VP potential[23] and the SE potential of Flambaum and Ginges,[25] added to the Dirac–Coulomb–Gaunt (DCG) Hamiltonian. For correlated calculations, we employed the molecular mean-field approximation Hamiltonian (X2Cmmf)[101] based on the DCG Hamiltonian, which we denote as $^2\text{DCG}^M$. In this approach, the converged Fock matrix obtained with the DCG Hamiltonian, with the effective QED potentials included, is exactly transformed to two-component form, that is, without any picture-change errors.[45–47] All basis sets were employed in uncontracted form with the small component generated by restricted kinetic balance (see Ref. 48 for details). Electronic structure analysis was carried out using projection analysis[91] where Pipek–Mezey localized MOs[91,102] are expanded in intrinsic, hence polarized, atomic orbitals.[103] The analysis was done at the molecular geometries optimized with respect to the employed Hamiltonian,

TABLE I. Calculated *ns* orbital energies in eV of group 1 and 11 elements from AOC-HF/dyall.v3z calculations based on the NR and DC Hamiltonians. The VP (Uehling) and SE (Flambaum–Ginges) corrections have been calculated as expectation values.

	NR	DC	VP	SE	ΔQED	SE/VP	SE/VP[123]	ΔQED/ΔR(%)
Li	−5.342	−5.343	-1.373×10^{-6}	4.092×10^{-5}	3.955×10^{-5}	−29.7949	−29.7058	−9.01
Na	−4.955	−4.962	-1.536×10^{-5}	2.950×10^{-4}	2.796×10^{-4}	−19.2057	−18.7963	−4.37
K	−4.013	−4.028	-3.423×10^{-5}	5.155×10^{-4}	4.813×10^{-4}	−15.0615	−14.7030	−3.19
Rb	−3.752	−3.811	-1.309×10^{-4}	1.361×10^{-3}	1.231×10^{-3}	−10.3981	−10.0783	−2.08
Cs	−3.365	−3.490	-2.989×10^{-4}	2.304×10^{-3}	2.005×10^{-3}	−7.7089	−7.4266	−1.61
Fr	−1.740	−3.611	-1.438×10^{-3}	6.333×10^{-3}	4.895×10^{-3}	−4.4038	−4.3351	−0.26
Uue	−2.993	−4.327	-1.034×10^{-2}	2.157×10^{-2}	1.123×10^{-2}	−2.0859	−4.3351	−0.84
Cu	−6.480	−6.649	-2.355×10^{-4}	2.840×10^{-3}	2.604×10^{-3}	−12.0606	−11.7316	−1.54
Ag	−5.985	−6.452	-7.342×10^{-4}	6.448×10^{-3}	5.714×10^{-3}	−8.7825	−8.4755	−1.22
Au	−6.003	−7.923	-4.635×10^{-3}	2.374×10^{-2}	1.910×10^{-2}	−5.1219	−4.9912	−1.00
Rg	−5.441	−11.425	-3.251×10^{-2}	8.408×10^{-2}	5.157×10^{-2}	−2.5863	−2.7223	−0.86

except for DCG with effQED, where the DCG structures were employed.

For the atomic calculations reported in Table I we employed Dyall v3z basis sets;[104–109] the basis set for Uue was specially optimized by Dyall for this work.[110]

For van der Waals dimers, the following orbitals were correlated: 5*d*6*s* for Hg, 5*d*6*s*6*p* for Rn, 6*d*7*s* for Cn, and 6*d*7*s*7*p* for Og. We used a virtual energy cutoff of 40 E_h. Dyall cv3z basis sets,[106–108] designed for core-valence correlation, were employed for the Hg and Cn species, whereas Dyall acv3z basis sets,[111–113] where the Dyall cv3z basis sets have been augmented by diffuse functions, were employed for Rn and Og species. Electronic structure calculations were done at the level of coupled-cluster singles-and-doubles with approximate triples correction [CCSD(T)] using the RELCCSD module.[114] We used the counterpoise correction[115] to minimize basis set superposition errors (BSSEs).

For the calculations of gold cyanide, we used the CCSD(T) method for comparison with experiment. In the CCSD(T) calculation, 4*f*5*s*5*p*5*d*6*s* for Au and all electrons of C and N were correlated, which is the same level as the previous work.[116] Dyall ae3z and ae4z basis sets,[106,107,109] designed for correlation of all electrons, were employed in the calculations. We employed a virtual energy cutoff of about 50 E_h and 80 E_h for dyall.ae3z and dyall.ae4z, respectively, which ensures that the correlating *h* and *i* orbitals, respectively, are included. Effective QED potentials for C and N atoms were not used, as explained in Sec. III. The potential energy surface (PES) was calculated in the vicinity of the equilibrium structure with a total of 49 points for each basis set, using internal coordinates r_1 (Au–C distance), r_2 (C–N distance). The bond angle was fixed at $\theta = 180°$. The step size for bond distances was 0.1 a_0. The surface fitting and determination of the equilibrium structure were carried out using the SURFIT program,[117] with convergence 3.2×10^{-10} or better on the gradient. In addition, to estimate the relativistic effects, we employed the two-component nonrelativistic (by using .NONREL keyword), 4c-scalar relativistic,[118,119] and the Dirac–Coulomb Hamiltonians at the density functional theory (DFT) level. In these calculations, we employed the B3LYP functional[120,121] and the dyall.3zp basis sets.[106,107,109]

For the calculation of Pb and Fl hydrides, the DCG Hamiltonian with and without effective QED potentials, as well as the Lévy-Leblond (LL)[119,122] Hamiltonian were employed. The dyall.3zp basis sets were used for all the elements. The B3LYP functional was used for both the projection analysis and the geometry optimization.

V. RESULTS

A. Atomic calculations

In Table I, we show the results of atomic calculations using average-of-configuration (AOC) HF,[124,125] which can be directly compared with Table I of Ref. 17 and which provide estimates for the valence-level Lamb shift for group 1 and 11 metal atoms. Pyykkö *et al.* focused on $ns_{1/2}$ orbital energies for estimating ionization energies, albeit, as pointed out by Thierfelder and Schwerdtfeger,[89] for Roentgenium ($Z = 111$), the first ionization is out of the $6d_{5/2}$ orbital. The VP and SE contributions come with opposite sign and are dominated by the latter.[123] However, the ratio SE/VP decreases significantly with increasing nuclear charge and, indeed, VP is predicted to eventually overtake SE at very high nuclear charges.[89] Pyykkö *et al.* calculated the SE contribution as $\langle V^U \rangle * (\mathrm{SE/VP})$, where (SE/VP) is the ratio for $2s_{1/2}$ of the corresponding hydrogen-like systems, including the nuclear-size effect, tabulated for $1 \le Z \le 100$ by Johnson and Soff[123] (a more recent compilation is provided by Yerokhin and Shabaev[126]). As confirmed by later calculations[127] and the numbers in Table I, this is a rather reasonable approximation.

Comparing relativistic and QED effects, one sees that the latter corrects the former by about −1% for the heavier atoms. For the gold atom, it is exactly so. In Table II, we show the effect of relativity and QED on all orbital energies of the gold atom. Two combinations of effective QED potentials have been used in variational calculations: The Uehling (U) VP potential has been combined either with the Flambaum–Ginges (FG) or Pyykkö–Zhao SE potentials. One sees that for both combinations of effective QED potentials, the relativistic effects are, with very few exceptions, reduced with a few percent. For $s_{1/2}$ orbitals, the difference in QED shift between the U+FG

TABLE II. Relativistic and QED effects on the orbital energies $\varepsilon(E_h)$ of the Au atom at the B3LYP/dyall.3zp level. The Uehling VP potential has been combined with two different SE potentials: FG (Flambaum–Ginges) and PZ (Pyykkö–Zhao) in variational calculations. Numbers in parentheses show the percentage-wise ratio ΔQED/ΔR for each combination of effective QED potentials.

	NR	DCG	Δ(U+FG)		Δ(U+PZ)	
$1s_{1/2}$	−2689.451	−2955.841	6.377×10^{00}	(−2.39)	6.243×10^{00}	(−2.34)
$2s_{1/2}$	−449.932	−523.020	8.448×10^{-1}	(−1.16)	8.586×10^{-1}	(−1.17)
$2p_{1/2}$	−432.492	−500.523	5.895×10^{-2}	(−0.09)	5.955×10^{-2}	(−0.09)
$2p_{3/2}$	−432.492	−433.755	1.194×10^{-1}	(−9.45)	-3.055×10^{-2}	(2.42)
$3s_{1/2}$	−105.753	−123.999	1.862×10^{-1}	(−1.02)	1.924×10^{-1}	(−1.05)
$3p_{1/2}$	−97.515	−114.096	7.320×10^{-3}	(−0.04)	1.462×10^{-2}	(−0.09)
$3p_{3/2}$	−97.515	−99.311	2.213×10^{-2}	(−1.23)	-8.516×10^{-3}	(0.47)
$3d_{3/2}$	−82.165	−83.236	-1.430×10^{-2}	(1.34)	-9.090×10^{-3}	(0.85)
$3d_{5/2}$	−82.165	−80.090	-5.817×10^{-3}	(−0.28)	-8.587×10^{-3}	(−0.41)
$4s_{1/2}$	−22.559	−27.178	4.650×10^{-2}	(−1.01)	4.833×10^{-2}	(−1.05)
$4p_{1/2}$	−18.993	−22.979	1.124×10^{-3}	(−0.03)	3.336×10^{-3}	(−0.08)
$4p_{3/2}$	−18.993	−19.424	4.651×10^{-3}	(−1.08)	-2.427×10^{-3}	(0.56)
$4d_{3/2}$	−12.440	−12.630	-3.439×10^{-3}	(1.82)	-2.307×10^{-3}	(1.22)
$4d_{5/2}$	−12.440	−11.971	-1.648×10^{-3}	(−0.35)	-2.185×10^{-3}	(−0.47)
$4f_{5/2}$	−3.648	−3.228	-2.383×10^{-3}	(−0.57)	-1.461×10^{-3}	(−0.35)
$4f_{7/2}$	−3.648	−3.091	-1.824×10^{-3}	(−0.33)	-1.425×10^{-3}	(−0.26)
$5s_{1/2}$	−3.253	−4.116	9.003×10^{-3}	(−1.04)	9.430×10^{-3}	(−1.09)
$5p_{1/2}$	−2.108	−2.745	-4.569×10^{-5}	(0.01)	4.105×10^{-4}	(−0.06)
$5p_{3/2}$	−2.108	−2.139	5.619×10^{-4}	(−1.82)	-5.703×10^{-4}	(1.85)
$5d_{3/2}$	−0.346	−0.333	-4.662×10^{-4}	(−3.61)	-3.486×10^{-4}	(−2.70)
$5d_{5/2}$	−0.346	−0.276	-2.881×10^{-4}	(−0.41)	-3.206×10^{-4}	(−0.46)
$6s_{1/2}$	−0.148	−0.205	6.519×10^{-4}	(−1.14)	6.726×10^{-4}	(−1.18)

and U+PZ combinations is below 5%; for other orbitals, the difference is generally larger. We note in particular that the shifts have systematically opposite sign for $p_{3/2}$ orbitals. Not surprisingly, the largest absolute shifts are observed for inner core orbitals, whereas the largest relative shift—0.33%—is seen for the $6s_{1/2}$ orbital.

In Table III, we show QED shifts of orbital energies, this time obtained perturbatively as expectation values. Compared to the shifts obtained from variational inclusion of the effective QED potentials, the largest absolute deviations concern the inner core orbitals. The smallest relative deviations are observed for $s_{1/2}$ orbitals and decreasing toward core. The larger relative deviations, on the other hand, are seen for p orbitals; the largest relative deviation concerns $5p_{1/2}$, but this can probably be attributed to noise since the QED shift on the energy of this orbital is particularly small with both combinations of effective QED potentials.

Table III also shows perturbative QED shifts of orbital energies obtained with the X2C Hamiltonian. When the effective QED potentials have been correctly picture-change transformed, deviations from the parent 4c calculation are below 3%, which clearly validates the use of these potentials in two-component relativistic calculations. On the other hand, without picture-change, significant errors are observed; the average unsigned error for U+FG and U+PZ is 130% and 47%, respectively. This is possibly worrisome since the U+PZ combination, expressed in terms of Gaussians, have been used without picture-change in scalar DKH calculations by Peterson and co-workers.[33–36]

B. Gold cyanide

In 2008, Zaleski-Ejgierd *et al.* reported CCSD(T)/cc-pVQZ calculations on the noble metal cyanides (MCN, M = Cu, Ag, Au).[128] Small-core scalar relativistic effective core potentials (SRECPs)[131] were used for the metal atoms and spin–orbit corrections added at the PBE-ZORA/QZ4P level. In 2013, Hill *et al.* reported CCSD(T)-F12/cc-pV5Z calculations on the same compounds by using the same SRECPs as the previous authors and adding a number of corrections.[116] As seen from Table IV, the newer calculations brought the M–C bond lengths of CuCN and AgCN in better agreement with experiment, but they increased the gap between theory and experiment for AuCN. This led Pyykkö to conjecture that this could be the first evidence of the effect of QED on molecular structure.[50]

To possibly verify this conjecture, we first carried out exploratory calculations at the B3LYP/dyall.3zp level. Table V shows the effects of relativity and QED on orbital sizes of the gold atom. For the valence $6s_{1/2}$, we observe an impressive relativistic contraction of 28.53 pm, whereas QED leads to an orbital expansion of 0.25 pm, roughly −1% of the relativistic effect.

We next turn to the AuCN molecule. We first, in Table VI, report bonding analysis in localized orbitals.[91] One finds a single σ-type Au–C bond, dominated by carbon $2s_{1/2}$ and gold $6s_{1/2}$, as well as a triple C–N bond. Equilibrium bond lengths r_e with respect to different Hamiltonians are reported in Table VII. We see a very significant scalar relativistic bond length contraction

TABLE III. First-order QED effects on the orbital energies $\varepsilon(E_h)$ of the Au atom at the B3LYP/dyall.3zp level using the DCG Hamiltonian or the X2C Hamiltonian, the latter with or without picture-change (PC) transformation. The Uehling VP potential has been combined with two different SE potentials: FG (Flambaum–Ginges) and PZ (Pyykkö–Zhao). Numbers in parentheses shows the percentage-wise ratio ΔQED/Δ for each combination of effective QED potentials.

	DCG		X2C - PC		X2C - noPC	
	Δ(U+FG)	Δ(U+PZ)	Δ(U+FG)	Δ(U+PZ)	Δ(U+FG)	Δ(U+PZ)
$1s_{1/2}$	6.620×10^{00}	6.465×10^{00}	6.632×10^{00}	6.477×10^{00}	7.522×10^{00}	8.253×10^{00}
$2s_{1/2}$	9.003×10^{-1}	9.022×10^{-1}	9.012×10^{-1}	9.030×10^{-1}	1.079×10^{00}	1.175×10^{00}
$2p_{1/2}$	1.184×10^{-1}	1.051×10^{-1}	1.187×10^{-1}	1.047×10^{-1}	1.971×10^{-1}	3.608×10^{-2}
$2p_{3/2}$	1.671×10^{-1}	4.922×10^{-3}	1.682×10^{-1}	5.005×10^{-3}	1.279×10^{-1}	6.342×10^{-3}
$3s_{1/2}$	2.016×10^{-1}	2.040×10^{-1}	2.020×10^{-1}	2.043×10^{-1}	2.441×10^{-1}	2.665×10^{-1}
$3p_{1/2}$	2.357×10^{-2}	2.674×10^{-2}	2.359×10^{-2}	2.665×10^{-3}	3.939×10^{-2}	9.351×10^{-3}
$3p_{3/2}$	3.554×10^{-2}	1.335×10^{-3}	3.574×10^{-2}	1.357×10^{-3}	2.671×10^{-2}	1.727×10^{-3}
$3d_{3/2}$	-1.234×10^{-3}	1.064×10^{-5}	-1.220×10^{-3}	1.066×10^{-5}	3.906×10^{-3}	3.605×10^{-7}
$3d_{5/2}$	6.494×10^{-3}	-1.680×10^{-7}	6.528×10^{-3}	-1.675×10^{-7}	3.296×10^{-3}	-1.132×10^{-7}
$4s_{1/2}$	5.082×10^{-2}	5.151×10^{-2}	5.097×10^{-2}	5.166×10^{-2}	6.173×10^{-2}	6.741×10^{-2}
$4p_{1/2}$	5.631×10^{-3}	6.658×10^{-3}	5.638×10^{-3}	6.637×10^{-3}	9.363×10^{-3}	2.339×10^{-3}
$4p_{3/2}$	8.392×10^{-3}	3.315×10^{-4}	8.444×10^{-3}	3.370×10^{-4}	6.292×10^{-3}	4.295×10^{-4}
$4d_{3/2}$	-1.331×10^{-4}	2.846×10^{-6}	-1.299×10^{-4}	2.851×10^{-6}	9.447×10^{-4}	9.962×10^{-8}
$4d_{5/2}$	1.461×10^{-3}	-4.294×10^{-8}	1.468×10^{-3}	-4.277×10^{-8}	7.944×10^{-4}	-2.822×10^{-8}
$4f_{5/2}$	-2.785×10^{-4}	-1.968×10^{-10}	-2.782×10^{-4}	-1.974×10^{-10}	1.089×10^{-5}	-1.184×10^{-10}
$4f_{7/2}$	2.190×10^{-4}	-9.047×10^{-11}	2.194×10^{-4}	-9.111×10^{-11}	9.735×10^{-6}	-9.557×10^{-11}
$5s_{1/2}$	1.001×10^{-2}	1.015×10^{-2}	1.004×10^{-2}	1.018×10^{-2}	1.217×10^{-2}	1.329×10^{-2}
$5p_{1/2}$	9.658×10^{-4}	1.152×10^{-3}	9.668×10^{-4}	1.149×10^{-3}	1.605×10^{-3}	4.052×10^{-4}
$5p_{3/2}$	1.373×10^{-3}	5.478×10^{-5}	1.382×10^{-3}	5.572×10^{-5}	1.029×10^{-3}	7.103×10^{-5}
$5d_{3/2}$	-1.078×10^{-5}	2.580×10^{-7}	-1.048×10^{-5}	2.582×10^{-7}	8.410×10^{-5}	9.077×10^{-9}
$5d_{5/2}$	1.216×10^{-4}	-3.635×10^{-9}	1.222×10^{-4}	-3.618×10^{-9}	6.669×10^{-5}	-2.375×10^{-9}
$6s_{1/2}$	7.888×10^{-4}	8.001×10^{-4}	7.908×10^{-4}	8.020×10^{-4}	9.586×10^{-4}	1.047×10^{-3}

of 25.31 pm, which is on par with the $6s_{1/2}$ orbital contraction observed in Table V. When going from a spin-free (SF) Hamiltonian to the Dirac–Coulomb one, one finds a further contraction of 0.29 pm, which agrees very well with the spin–orbit correction of −0.28 pm obtained by Hill *et al.* taking the same difference, albeit at the CCSD(T) level.[116] However, this contraction is almost canceled when adding the Gaunt term, which brings spin-other-orbit interaction[3] and which was not considered by Hill *et al.*[116] At this level of theory, the total relativistic effect on the bond length is thereby −25.38 pm; in a future work, we hope to assert the effect of replacing the Gaunt term by the full Breit one. Finally, adding QED effects, we observe a bond length extension of 0.19 pm, −0.75% of the relativistic effect. One may note that the QED effect is of the same order as the effect of adding the Gaunt term.[89] In passing, we note from Table VII that incorporation of QED effects through the atomic shift operator (ASHIFT) described in Sec. II C also leads to a bond extension, albeit only capturing half of the full QED effect.

To obtain more accurate bond lengths, we proceeded as indicated in Table VIII: ^{2}DCG^M-CCSD(T) calculations were carried out in the Dyall ae3z and ae4z basis sets and then extrapolated to the

TABLE IV. M–C bond lengths (in pm) in MCN (M = Cu, Ag, Au) from microwave (MW) spectroscopy and calculations.

	CuCN	AgCN	AuCN	
r_0	183.231(7)	203.324(45)	191.251(16)	MW[a]
r_s	183.284(4)	203.4182(27)	191.225 19(84)	MW[a]
r_e	182.36	202.42	191.05	Calc.[128]
r_e	182.65	202.99	190.71	Calc.[116]

[a]CuCN: Ref. 129. AgCN, AuCN: Ref. 130.

TABLE V. Relativistic and QED effects on the rms radius $\langle r^2 \rangle^{1/2}$(pm) of the Au atom at the B3LYP/dyall.3zp level. Effective QED potentials: VP(Uehling) + SE(Flambaum–Ginges).

	NR	DCG	DCG+QED	ΔR	ΔQED	ΔQED/ΔR (%)
$5s_{1/2}$	57.71	52.23	52.28	−5.48	0.05	−0.86
$5p_{1/2}$	63.16	56.78	56.78	−6.38	0.00	−0.02
$5p_{3/2}$	63.16	62.37	62.38	−0.80	0.01	−1.04
$5d_{3/2}$	91.07	90.81	90.78	−0.26	−0.03	10.46
$5d_{5/2}$	91.07	95.75	95.73	4.68	−0.02	−0.36
$6s_{1/2}$	196.07	167.54	167.79	−28.53	0.25	−0.88

TABLE VI. Gross populations obtained by projection analysis using Pipek–Mezey localized orbitals at the DCG/B3LYP/dyall.3zp level. $\langle\varepsilon\rangle$ is the expectation value in E_h with respect to the Kohn–Sham Hamiltonian.

		Au		C			N		
ω	$\langle\varepsilon\rangle$	$5d_{5/2}$	$6s_{1/2}$	$2s_{1/2}$	$2p_{1/2}$	$2p_{3/2}$	$2s_{1/2}$	$2p_{1/2}$	$2p_{3/2}$
3/2	−0.342	−0.01	0.00	0.00	0.00	0.92	0.00	0.00	1.09
1/2	−0.345	0.00	0.00	0.00	0.65	0.28	0.00	0.64	0.43
1/2	−0.586	0.15	0.39	0.92	0.17	0.34	0.01	−0.01	−0.02
1/2	−0.781	0.00	0.01	0.24	0.12	0.38	0.15	0.44	0.65

TABLE VII. Equilibrium bond lengths r_e (in pm) of AuCN calculated at the B3LYP/dyall.3zp level using various Hamiltonians. Numbers in parentheses indicate the change with respect to the previous line, except ASHIFT, which refers to DCG. SF refers to a spin-free four-component relativistic Hamiltonian.

Hamiltonian	Au–C	C–N
NR	218.54	115.71
SF	193.23 (−25.31)	115.54 (−0.17)
DC	192.94 (−0.29)	115.56 (+0.02)
DCG	193.16 (+0.22)	115.58 (+0.01)
QED	193.35 (+0.19)	115.57 (+0.00)
ASHIFT	193.25 (+0.09)	115.58 (+0.00)

basis set limit,[132] indicated by "ae∞z." We then added the triples ΔT and quadruples ΔQ corrections reported by Hill *et al.*[116] to obtain a Au–C bond length of 190.75 pm, very close to the value 190.71 pm reported by Peterson and co-workers. Finally, we add a QED correction of 0.19 pm, identical to what we obtained at the B3LYP/dyall.3zp level, to obtain our final value of 190.99 pm.

The devil is, however, in the details: Our Born–Oppenheimer equilibrium bond lengths r_e are not directly comparable to the structural parameters extracted from the rotational spectra recorded by Okabayashi *et al.*[130] Experiment gives access to rotational constants B_v for individual vibrational states. For a linear molecule like AuCN, the rotational constant, in units of frequency, is expressed as

$$B = \frac{\hbar}{4\pi I_\perp}; \quad I_\perp = I_{xx} = I_{yy} = \sum_A m_A z_A^2, \tag{42}$$

TABLE VIII. Final, recommended equilibrium Au–C bond length r_e (pm) at the ^{2}DCG^M-CCSD(T) level for the AuCN molecule. ΔQED is the difference between the extrapolated basis set limit ae∞z with QED and without QED.

	Au–C	C–N
ae3z	190.89	116.66
ae4z	190.70	116.28
ae∞z	190.58	116.07
ΔT[116]	0.26	−0.10
ΔQ[116]	−0.09	0.19
Final w/o QED	190.75	116.16
ΔQED	0.19	0.00
Final	190.94	116.16

when the molecular axis is aligned with the z-axis. z_A is the distance of atom A from the center of mass. Both the effective r_0 and substitution r_s structures are obtained by assuming identical structures for all isotopomers of the target molecule observed in experiment.[133,134] Effective structures r_0 are obtained by least-square fitting of experimental ground-state inertial moments, whereas substitution structures r_s are obtained from observation of how rotational constants (and center of mass) change upon single isotope substitution $A \to A'$. For a linear molecule, one has

$$|z_A| = \sqrt{\frac{\hbar}{4\pi\mu}\left(\frac{1}{B^{A'}} - \frac{1}{B^A}\right)}; \quad \frac{1}{\mu} = \frac{1}{M} + \frac{1}{\Delta m_A}, \tag{43}$$

where M is the total mass of the parent isotopomer. In the case of AuCN, $|z_C|$ and $|z_N|$ could be estimated from corresponding single isotope substitutions. However, since gold has a single naturally occurring isotope, ^{197}Au, $|z_{Au}|$ was obtained from the definition of center of mass.[135]

Empirically, one typically finds $r_0 \geq r_s \geq r_e$,[134] which suggests that we should rather compare our recommended r_e = 190.99 pm for Au–C with the corresponding substitution bond length r_s = 191.225 19(84) pm reported by Okabayashi *et al.*[130] However, a better comparison is provided by calculating the ground-state rotational constant B_0 from B_e. From perturbation theory, excluding Fermi resonances, the rotational constant for a given vibrational state v of a general molecule is related to B_e as follows:[134]

$$B_v^\xi = B_e^\xi - \sum_i \alpha_i^\xi \left(v_i + \frac{d_i}{2}\right) + \frac{1}{2}\sum_{i,j} \gamma_{i,j}^\xi \left(v_i + \frac{d_i}{2}\right)\left(v_j + \frac{d_j}{2}\right) + \cdots. \tag{44}$$

Here, ξ is the axis of rotation, α^ξ and γ^ξ are vibration and rotation interaction constants of different orders, and d_i is the degeneracy of vibration mode i. The series generally converges rapidly, and for AuCN, a suitable expression is therefore given by

$$B_0 \approx B_e - \frac{1}{2}[\alpha_{100} + \alpha_{001} + 2\alpha_{01^10}], \tag{45}$$

using the notation $\alpha_{v_1 v_2 v_3}$, where v_1 corresponds to the C–N stretch, v_2 to the doubly degenerate bending mode, and v_3 to the Au–C stretch.

Hill *et al.*[116] carried out both perturbative and variational rovibrational calculations. Using their calculated potential surfaces,[136] we have extracted vibration–rotation interaction constants $\alpha_{v_1 v_2 v_3}$. Combined with our best equilibrium structures from Table VIII,

TABLE IX. Calculated and experimental rotational constants (in MHz) for AuCN.

	$^{197}Au^{12}C^{14}N$	$^{197}Au^{13}C^{14}N$	$^{197}Au^{12}C^{15}N$
α_1	14.55	13.53	14.06
α_2	−10.98	−10.25	−10.59
α_3	12.17	11.91	11.30
	w/o QED		
B_e	3237.5	3184.5	3086.4
B_0	3235.1	3182.1	3084.3
	With QED		
B_e	3232.8	3179.9	3082.0
B_0	3230.4	3177.5	3079.9
B_0 (expt.)[130]	3230.211 15(18)	3177.207 93(13)	3079.735 40(12)

we have calculated the rotational constants of the ground vibrational state of the three isotopomers of AuCN studied by Okabayashi *et al.*[130] As can be seen from Table IX, the inclusion of QED corrections brings about a dramatic improvement with respect to experiment. Not surprisingly then, extraction of substitution structures by the same procedure as Okabayashi *et al.*,[130] correcting for Lamb shift effects, brings our calculated substitution bond lengths within 0.05 pm of the experimental ones (cf. Table X). We expect further refinement of the potential surface to improve agreement with experiment; we note for instance that our calculated vibration–rotation interaction constant associated with bending for the most abundant isotopomer $^{197}Au^{12}C^{14}N$ is −10.98 MHz, compared to −11.9781 MHz when extracted from experiment.[116]

C. van der Waals dimers

As a second molecular application of our implementation, we consider spectroscopic constants of dimers with van der Waals bonding (M_2, M = Hg, Rn, Cn, Og). In Table XI, we report our calculated equilibrium bond lengths r_e, harmonic frequencies ω_e, anharmonic constants $\omega_e x_e$, and dissociation energies D_e for these species. We see that the QED effect on bond length is on the order of 0.15 pm for row-6 dimers and approximately doubles when going to the superheavy elements; for Og_2, the QED bond length extension is in line with what was reported by Hangele and Dolg using relativistic effective core potentials.[40] The QED effect on dissociation energies is rather small: on the order of 0.4% for the superheavy dimers.

D. Reaction energies: Pb and Fl hydrides

As a final case study, we consider the reaction energy of $XH_4 \longrightarrow XH_2 + H_2$ to which Dyall *et al.* proposed that the Lamb shift could make a chemically significant contribution.[53] Their argument was based on the observation that QED effects are most important for s orbitals, as seen in Tables II and V, and that this is a reaction with a significant change of the valence s population of a heavy element. We have investigated this at the B3LYP/dyall.3zp level and also included the corresponding reaction involving the heavier homologue flerovium. Optimized equilibrium structures are given in Table XII. For the tetrahydrides, we assumed T_d symmetry, in line with experiment[137] (PbH_4) and previous calculation[138] (FlH_4).

To monitor valence s populations, we carried out bonding analysis in Pipek–Mezey localized MOs.[91,102] From Table XIII, the change of the valence s population from XH_4 to XH_2 is 0.45 and 0.30 for Pb and Fl systems, respectively. From Table XIV, one sees that in the tetrahydrides, the valence s population is contained in the four σ_{XH} bonds. In contrast, in the dihydrides, the two σ_{XH} bonds are mediated by the valence *p* orbitals of the metals, and most of the valence s population is found in a nonbonding (nb) orbital.

TABLE X. Calculated and experimental substitution structure (in pm) for AuCN.

	r_s(Au–C)	r_s(C–N)
w/o QED	190.991	115.910
With QED	191.184	115.909
Expt.[130]	191.225 19(84)	115.865 45(97)

TABLE XI. Spectroscopic constants of heavy group 12 and 18 dimers obtained at the $^2DCG^M$-CCSD(T) level using the U+FG combination of effective QED potentials and either dyall.cv3z (Hg_2,Cn_2) or dyall.acv3z (Rn_2,Og_2) basis sets. Numbers in parentheses indicate the QED effect.

	r_e (pm)	ω_e (cm^{-1})	$\omega_e x_e$ (cm^{-1})	D_e (cm^{-1})
Hg_2	385.71	16.65	0.232	277.7
	(0.15)	(−0.03)	(−0.002)	(−0.02)
Cn_2	354.75	22.95	0.255	532.7
	(0.36)	(−0.11)	(0.001)	(−2.78)
Rn_2	463.60	13.79	0.286	174.9
	(0.14)	(−0.02)	(-1.0×10^{-04})	(−0.41)
Og_2	449.97	17.10	0.210	391.1
	(0.28)	(−0.04)	(0.001)	(−1.32)

TABLE XII. Optimized equilibrium structures of Pb and Fl hydrides at the B3LYP/dyall.3zp level based on the DCG Hamiltonian. r_e and α_e refer to the X–H bond length (Å) and H–X–H angle (deg), respectively.

	PbH_2		FlH_2		PbH_4	FlH_4
	r_e	α_e	r_e	α_e	r_e	r_e
NR	1.879	90.83	2.017	90.85	1.816	1.959
DCG	1.845	91.18	1.920	93.35	1.756	1.825

TABLE XIII. Charge *Q* and electronic configurations of Pb and Fl atoms in the title compounds obtained by projection analysis at the B3LYP/dyall.3zp level.

	Q	Atomic configuration
PbH_2	0.39	$5d_{3/2}^{4.00}$ $5d_{5/2}^{5.99}$ $6s_{1/2}^{1.86}$ $6p_{1/2}^{0.90}$ $6p_{3/2}^{0.86}$
PbH_4	0.66	$5d_{3/2}^{3.99}$ $5d_{5/2}^{5.98}$ $6s_{1/2}^{1.41}$ $6p_{1/2}^{0.85}$ $6p_{3/2}^{1.10}$
FlH_2	0.32	$6d_{3/2}^{3.99}$ $6d_{5/2}^{5.97}$ $7s_{1/2}^{1.91}$ $7p_{1/2}^{1.26}$ $7p_{3/2}^{0.55}$
FlH_4	0.46	$6d_{3/2}^{3.98}$ $6d_{5/2}^{5.94}$ $7s_{1/2}^{1.61}$ $7p_{1/2}^{1.17}$ $7p_{3/2}^{0.84}$

TABLE XIV. Gross population obtained by projection analysis of the localized bonding orbitals in the title compounds at the B3LYP level based on the DCG Hamiltonian. $\langle\varepsilon\rangle$ refers to the expectation value with respect to the Kohn–Sham Hamiltonian (in E_h).

		X							H_i
		$\langle\varepsilon\rangle$	$5s_{1/2}$	$5d_{3/2}$	$5d_{5/2}$	$6s_{1/2}$	$6p_{1/2}$	$6p_{3/2}$	$1s_{1/2}$
PbH_4	σ_{XH_i}	−0.4192		0.00	0.00	0.35	0.21	0.27	1.19
PbH_2	σ_{XH_i}	−0.3384	0.00	0.00	0.00	0.03	0.37	0.37	1.24
	nb	−1.0182	0.13	0.00	0.00	1.62	0.14	0.11	−0.03
		$\langle\varepsilon\rangle$	$6s_{1/2}$	$6d_{3/2}$	$6d_{5/2}$	$7s_{1/2}$	$7p_{1/2}$	$7p_{3/2}$	$1s_{1/2}$
FlH_4	σ_{XH_i}	−0.4524		0.00	0.01	0.40	0.27	0.20	1.11
FlH_2	σ_{XH_i}	−0.3469	0.00	0.00	0.01	0.03	0.52	0.25	1.18
	nb	−1.2235	0.11	0.04	0.06	1.57	0.15	0.04	−0.03

TABLE XV. Reaction energy of $PbH_4 \rightarrow PbH_2 + H_2$ (in kcal/mol). ΔDCG refers to the difference between DCG and NR. Other Δ refers to the difference from the DCG value.

	QED effect	Reac. energy	Δ (kcal/mol)	Δ (%)
NR	None	16.47		
DCG	None	−8.99	−25.46	
	VP	−9.09	−0.10	0.41
	SE	−8.56	0.42	−1.67
	VP+SE	−8.66	0.32	−1.27
	VP+SE(ASHIFT[a])	−8.97	0.02	−0.07
	VP+SE(ASHIFT[b])	−9.06	−0.08	0.31

[a]Occupation of atomic fragment was $6s^2 6p^2$.
[b]Using the occupations of Table XIII.

Turning next to Tables XV and XVI, we see that both reactions are endothermic at the nonrelativistic level, but they become clearly exothermic with the addition of relativistic effects. For Pb, QED reduces the relativistic effect by 1.25%. Its value is 0.32 kcal/mol, which is at the lower end of the perturbation estimate of Dyall *et al.*[53] For Fl, QED reduces the relativistic effect by 0.50%. Interestingly, its value is very close to that for the Pb reaction, despite Fl being a much heavier atom. The reason for this unexpected result is the cancelation between the SE and VP effects. From Tables XV and XVI, the ratio of VP and SE is ∼1:−4.2 for the Pb system, while it is ∼1:−1.8 for the Fl system. Discussion along these lines is also found in Refs. 55 and 89. Finally, we note from Tables XV and XVI that the atomic shift operator (ASHIFT), either using atomic ground-state occupations or the effective atomic configuration in the molecules given in Table XIII, is not reliable for describing QED effects in molecules.

TABLE XVI. Reaction energy of $FlH_4 \rightarrow FlH_2 + H_2$ (in kcal/mol). ΔDCG refers to the difference between DCG and NR. Other Δ refers to the difference from the DCG value.

	QED effect	Reac. Energy	Δ (kcal/mol)	Δ (%)
NR	None	9.52		
DCG	None	−60.02	−69.54	
	VP	−60.43	−0.41	0.59
	SE	−59.27	0.75	−1.08
	VP+SE	−59.67	0.35	−0.50
	VP+SE(ASHIFT[a])	−60.10	−0.07	0.10
	VP+SE(ASHIFT[b])	−60.23	−0.21	0.30

[a]Occupation of the atomic fragment was $7s^2 7p^2$.
[b]Using the occupations of Table XIII.

VI. CONCLUSIONS

We have implemented effective QED potentials for relativistic molecular calculations by grafting code from the numerical atomic code GRASP onto the DFT grid of DIRAC. A general disadvantage of numerical integration is a higher computational cost than that involved in analytical evaluation, to the extent that such expressions are available, although the implementation itself is easier and considerable savings are achieved by the locality of the effective QED potentials.

We report several applications of the new code, mostly using the molecular mean-field approximation Hamiltonian (X2Cmmf). We demonstrate (Table II) that with proper picture-change transformation of the effective QED potentials, our two-component relativistic results reproduce the four-component reference data remarkably well. On the other hand, this transformation is mandatory since the picture-change errors are sizable.

We confirm that the discrepancy between the accurate calculations of Hill *et al.*[116] and experiment[130] is due to QED by directly calculating the ground-state rotational constants B_0 for the isotopomers investigated in the MW experiment. We then find that QED reduces the discrepancy of the corresponding substitution Au–C bond length r_s from 0.23 to 0.04 pm with respect to experiment.

For the rare-gas dimers Hg_2 and Rn_2, we find that QED increases bond lengths by about 0.15 pm. For the superheavy homologues, the bond length increase is on the order of 0.30 pm; the effect on dissociation energies is rather small (∼0.4%).

We have also investigated the effect of QED on the reaction energy of $XH_4 \longrightarrow XH_2 + H_2$ (X = Pb, Fl). From projection analysis, we do find that there is a significant change of valence s population of the metals during the reaction, in line with the proposition of

Dyall *et al.*[53] Interestingly, though, we also find that the valence s population essentially resides in bonding orbitals in the tetrahydrides, but it resides in nonbonding ones in the case of dihydrides. We find for the dissociation of lead tetrahydride that QED reduces the magnitude of the reaction energy by 0.32 kcal/mol (−1.27%); for the superheavy homologue, the magnitude of the QED effect is basically the same (0.35 kcal/mol). This possibly surprising observation is explained by the reduction of the (negative) SE/VP ratio with increasing nuclear charge.

For these metal hydrides, and also AuCN, we have also tried a simpler approach for the incorporation of QED effects in molecular calculations in the form of an atomic shift operator, but we find that this is not a reliable approach.

We would like to stress that our implementation of effective QED potential is general in the sense that they are available in all parts of the code. A natural continuation of our project will therefore be to explore the impact of these potentials on molecular properties by probing electron density in the vicinity of nuclei, where the QED effects are generated. Our results so far indicate that QED effects may be more important than for the valence properties reported in the present work. For instance, the QED effect on the parity violation energy of H_2Po_2 is 2.38%, although it depends on the choice of effective QED potentials.[139]

ACKNOWLEDGMENTS

This project received funding from the European Research Council (ERC) under the European Union's Horizon 2020 research and innovation program (Grant Agreement No. 101019907 HAMP-vQED) as well as from the Agence Nationale de la Recherche (Grant No. ANR-17-CE29-0004-01 molQED). A.S. acknowledges financial support from Japan Society for the Promotion of Science (JSPS) KAKENHI Grant Nos. 17J02767, 20K22553, and 21K1464 and JSPS Overseas Challenge Program for Young Researchers, Grant No. 201880193. The authors gratefully acknowledge the use of computing resources from CALMIP (Calcul en Midi-Pyrenes) and supercomputer of ACCMS (Kyoto University) and Research Institute for Information Technology, Kyushu University (General Projects). We would like to thank Kirk Peterson (Washington State), Toshiaki Okabayashi (Shizuoka), Pekka Pyykkö (Helsinki), Jacinda Ginges (Brisbane), and Radovan Bast (Tromsø) for valuable discussions.

AUTHOR DECLARATIONS

Conflict of Interest

The authors have no conflicts to disclose.

Author Contributions

The overall project was conceived and supervised by TS. All programming and calculations were carried out by AS, whereas MS is the main contributor to the theory sections, notably the appendix.

Ayaki Sunaga: Formal analysis (equal); Investigation (equal); Methodology (equal); Software (lead); Writing – original draft (equal). **Maen Salman**: Methodology (equal); Writing – original draft (equal). **Trond Saue**: Conceptualization (lead); Formal analysis (equal); Supervision (lead); Writing – original draft (equal).

DATA AVAILABILITY

The data that support the findings of this study are openly available in ZENODO at https://doi.org/10.5281/zenodo.6874728, see also Ref. 99. The DIRAC outputs contain information about the precise build of the corresponding executable and, most importantly, the git commit hash, which provides a unique identifier of the precise version of DIRAC generating the output, hence allowing reproduction of the results. We have also included the potential surface generated by Hill *et al.*[116] for AuCN, kindly made available by Kirk Peterson.

APPENDIX: THEORY BACKGROUND

Since we hope to reach a wider audience than QED specialists, we provide in this Appendix a compact, yet accessible, introduction (crash course) to QED that would otherwise have necessitated consulting disparate sources. More precisely, in this Appendix, we shall discuss the lowest-order BSQED corrections, and show how the effective potentials associated with these QED processes can be derived within the scattering matrix ($\mathcal{S}$-matrix) formalism. These effective potentials are to be used in practical relativistic calculations in order to account for the physics that is missing from the Dirac theory. In "conventional" QED, one studies how the free-electron field interacts with the free quantized electromagnetic field and/or with an potential source (the scattering problem). On the other hand, BSQED theory studies the same problem but with electrons that are already interacting with some time-independent external field, i.e., their wavefunctions are solutions to the bound-state Dirac equation instead of the free one. This is known as the Furry picture of quantum mechanics; see for instance Refs. 65 and 59 (Sec. 15g).

We shall use unbold symbols for four-quantities, such as space-time points (events): $x = (ct, \boldsymbol{x})$, here in contravariant coordinates, where $\boldsymbol{x}$ is the spatial position vector and the contravariant metric tensor $g^{\mu\nu} = \mathrm{diag}(+1, -1, -1, -1)$. The gamma matrices are defined through their anti-commutation relation

$$\gamma^\mu \gamma^\nu + \gamma^\nu \gamma^\mu = 2g^{\mu\nu}\mathbb{1}_4. \tag{A1}$$

In Dirac basis, they are represented by $\gamma^0 = \beta$ and $\boldsymbol{\gamma} = \beta\boldsymbol{\alpha}$. Following Lindgren,[73] we shall complement the Dirac $\boldsymbol{\alpha}$ matrices with $\alpha^0 = \mathbb{1}_4$ to form a pseudo-4-vector. We finally note that we put hats ($\hat{}$) on quantities that contain creation/annihilation operators acting on occupation number states. Contrary to conventional QED sources, we have decided to express the formalism in full SI units.

1. Electron field operator

The electron field operator is given by the following annihilation expansion over all solutions of the Dirac equation:

$$\hat{\Psi}(x) = \sum_i \psi_i(x) c_i, \text{ with } \psi_i(x) = \psi_i(\boldsymbol{x}) e^{-\frac{i}{\hbar}E_i t}. \tag{A2}$$

In this expression, c_i is the electron annihilation operator obeying the fermionic algebra relations,

$$\{c_i, c_j^\dagger\} = \delta_{ij}, \text{ and } \{c_i, c_j\} = \{c_i^\dagger, c_j^\dagger\} = 0, \tag{A3}$$

and associated with the i-th spatial wavefunction $\psi_i(\boldsymbol{x})$ and energy-level E_i that solve the time-independent Dirac equation

in the presence of a time-independent external four-potential $A^e = (\varphi^e/c, \boldsymbol{A}^e)$,

$$H_D \psi_i(\boldsymbol{x}) = E_i \psi_i(\boldsymbol{x}),$$

with

$$H_D = c\boldsymbol{\alpha} \cdot \left(-i\hbar\nabla + e\boldsymbol{A}^e(\boldsymbol{x})\right) - e\varphi^e(\boldsymbol{x}) + \beta m_e c^2. \tag{A4}$$

The electron vacuum state is defined to be the one that vanishes after any annihilation,

$$c_i|0_e\rangle = 0, \quad \forall i. \tag{A5}$$

In order to forbid the transition of positive-energy electrons to the negative-energy continuum by the Pauli exclusion principle and to obtain a stable atomic theory, Dirac[140] postulated that this continuum should be totally filled with electrons that are not observed (Dirac sea). This means that the vacuum state is redefined to be the state containing no positive-energy electrons and a fully occupied negative-energy electron sea. Dirac then argued that when a negative-energy electron absorbs enough energy ($E \geq 2m_e c^2$), it becomes real (observable) and leaves, for mass- and charge-conservation reasons, a positron behind (Dirac hole theory).[141] This last reasoning allows one to define[142]

$$\begin{aligned} c_i &= a_i, \qquad \text{for} \quad E_i > 0, \\ c_i &= b_i^\dagger, \qquad \text{for} \quad E_i < 0. \end{aligned} \tag{A6}$$

Here, operators a_i and b_i are introduced to distinguish between the particle (electron) and its hole (positron), and the second line indicates that the annihilation of a negative-energy electron with c_i is equivalent to the creation of a (positive-energy) hole (positron) with $b_i^\dagger$. The electron field operator of Eq. (A2) can be written, with respect to these definitions, as

$$\hat{\Psi}(x) = \sum_{E_i>0} \psi_i(x) a_i + \sum_{E_i<0} \psi_i(x) b_i^\dagger. \tag{A7}$$

Despite its experimental success in predicting the existence of the positron,[143] the hole theory (its physical implications) was, shortly after its introduction, abandoned. Many physicists including Pauli, Bohr, Weisskopf, Heisenberg, and Majorana opposed this theory, as clearly indicated in Refs. 144 (Sec. 1.6), 145, 146 (Sec. 4.4), and 147. This opposition came mainly from the following flaws of the Dirac hole theory: (1) the existence of a non-observable infinite negative energy and charge and (2) the fact that for massive boson systems, whose wavefunctions satisfy the Klein–Gordon equation, the Dirac argument would not hold and that the existence of these bosons is not justified. Modern quantum field theory reached the same mathematical expressions derived with respect to Dirac's hole theory but provided a more symmetric picture between electrons and positrons, in which (1) one only sees electrons and positrons with positive energies, (2) the infinite negative-energy electron sea assumption is no longer necessary, and (3) operators, such as the Hamiltonian, and charge are replaced by their normal-ordered forms. This physical interpretation leads to the modern definition of the vacuum state, one that obeys

$$a_i|0_e\rangle = b_i|0_e\rangle = 0, \quad \forall i \tag{A8}$$

and contains zero positive-energy electrons and positrons. To get a wider and more detailed vision of the historical development of the quantum field theory, the reader may consult Weinberg in Ref. 148 (Sec. 1.2 and Chap. 5) and Ref. 149, Mehra in Ref. 150 (Chap. 29), Schweber in Ref. 144, Kragh in Ref. 151, and Weisskopf in Ref. 152.

2. Photon field operator

The photon field operator is written as a sum over positive and negative plane-wave Fourier modes,

$$\hat{A}_\mu(x) = \hat{A}_\mu^+(x) + \hat{A}_\mu^-(x), \tag{A9}$$

$$\hat{A}_\mu^+(x) = \sum_{r=0}^{3} \sum_{\boldsymbol{k}} N_{\boldsymbol{k}} a(\boldsymbol{k}, r) \varepsilon_\mu(\boldsymbol{k}, r) e^{-ik\cdot x}, \tag{A10}$$

$$\hat{A}_\mu^-(x) = \sum_{r=0}^{3} \sum_{\boldsymbol{k}} N_{\boldsymbol{k}} a^\dagger(\boldsymbol{k}, r) \varepsilon_\mu(\boldsymbol{k}, r) e^{+ik\cdot x}, \tag{A11}$$

where $N_{\boldsymbol{k}} = \sqrt{\hbar/(2\epsilon_0 \omega_{\boldsymbol{k}} V)}$ is the normalization constant, the zeroth component four-wave vector is $k_0 = |\boldsymbol{k}| = \omega_{\boldsymbol{k}}/c$, $\varepsilon_\mu(\boldsymbol{k}, r)$ are the four polarization vectors, and $a(\boldsymbol{k}, r)$ [and $a^\dagger(\boldsymbol{k}, r)$] is the annihilation (creation) operator that annihilates (creates) a photon with wave vector $\boldsymbol{k}$ and polarization r, respectively {see Refs. 78 [Eqs. (5.16a)–(5.16c)] and 153 (Sec. 8.4)}. The choice of k_0 is imposed by the fact that the photon field operator must satisfy the Maxwell equation

$$\Box \hat{A}_\mu(x) = 0, \quad \text{with} \quad \Box = \frac{1}{c^2}\frac{\partial^2}{\partial t^2} - \nabla^2, \tag{A12}$$

obtained after setting the Lorenz gauge condition ($\partial^\mu \hat{A}_\mu = 0$) . This equation leads to the (massless) photon energy–momentum relation

$$k^2 = 0. \tag{A13}$$

The boson creation and annihilation operators do satisfy the following bosonic commutation relations:

$$\left[a(\boldsymbol{k}, r), a^\dagger(\boldsymbol{k}', s)\right] = \delta_{rs}\zeta_r \delta_{\boldsymbol{k},\boldsymbol{k}'}, \tag{A14}$$

$$\left[a^\dagger(\boldsymbol{k}, r), a^\dagger(\boldsymbol{k}', s)\right] = \left[a(\boldsymbol{k}, r), a(\boldsymbol{k}', s)\right] = 0. \tag{A15}$$

Here, ζ_r is a function defined by the following relation:

$$\zeta_r = \begin{cases} +1, & r = 0, \\ -1, & r = 1, 2, 3, \end{cases} \tag{A16}$$

and the polarization vectors satisfy the following completeness relation:

$$\sum_{r=0}^{3} \zeta_r \epsilon^\mu(\boldsymbol{k}, r) \epsilon^\nu(\boldsymbol{k}, r) = -g^{\mu\nu}. \tag{A17}$$

Finally, we note that the photon vacuum state is defined to be the state that satisfies the following relation:

$$\begin{aligned} &a(\boldsymbol{k}, r)|0_p\rangle = 0, \ \forall\ \boldsymbol{k}, r, \\ &\rightarrow \hat{A}_\mu^+(x)|0_p\rangle = 0, \ \forall\ \mu, x. \end{aligned} \tag{A18}$$

We shall now consider the interaction between the noninteracting electron and photon fields and show how one can derive QED corrections using perturbation theory.

3. Perturbation theory

As in conventional perturbation theory, one wants to get the eigen solutions of the following total Hamiltonian:

$$\hat{H}_S = \hat{H}_S^0 + \lambda \hat{H}_S^1. \tag{A19}$$

The zeroth-order Hamiltonian

$$\hat{H}_S^0 = \hat{H}_{\text{electron}}^0 + \hat{H}_{\text{photon}}^0 \tag{A20}$$

represents the free-electron and free photon fields. The electronic part is given by a spatial integral over the normal-ordered Dirac Hamiltonian density,

$$\begin{aligned}\hat{H}_{\text{electron}}^0 &= \int d^3x : \hat{\Psi}^\dagger(x) H_D(\boldsymbol{x}) \hat{\Psi}(x) : \\ &= \sum_{E_i>0} E_i a_i^\dagger a_i - \sum_{E_i<0} E_i b_i^\dagger b_i,\end{aligned} \tag{A21}$$

where in BSQED, H_D is the Dirac Hamiltonian in the presence of the external four-potential $A^e = (\varphi^e/c, \boldsymbol{A}^e)$, given in Eq. (A4), and where normal-ordering is indicated by double dots. The free photon Hamiltonian is written as an integral of the electromagnetic Hamiltonian density,

$$\begin{aligned}\hat{H}_{\text{photon}}^0 &= \frac{1}{\mu_0} \int d^3x : \Big[-(\partial^0 \hat{A}^\mu(x))(\partial_0 \hat{A}_\mu(x)) \\ &\quad + \frac{1}{2}(\partial^\nu \hat{A}^\mu(x))(\partial_\nu \hat{A}_\mu(x)) \Big] : \\ &= \sum_{\boldsymbol{k}} \sum_{r=0}^{3} \hbar \omega_{\boldsymbol{k}} \zeta_r a^\dagger(\boldsymbol{k}, r) a(\boldsymbol{k}, r).\end{aligned} \tag{A22}$$

For further details and discussions on the photon Hamiltonian, the reader may consult Greiner and Reinhardt in Ref. 61 (Sec. 7.3) and Mandl and Shaw in Ref. 78 (Chap. 5).

The perturbation Hamiltonian $\hat{H}_S^1$ complicates the problem and prevents us from obtaining eigen solutions of the full Hamiltonian $\hat{H}_S$. λ is a dimensionless parameter that can be varied between 0 and 1 and which keeps track of the perturbation order. This parameter is to be taken to be 1 in order to account for the full perturbation by the end of the calculation. Notice that so far, our Hamiltonians have an S subscript; this is made to indicate that they are in the Schrödinger picture of quantum mechanics. Assuming that we know the eigen solutions of the unperturbed time-independent problem equation

$$\begin{aligned}\hat{H}_S^0 \big|\Phi_0^\alpha\big\rangle_S &= E_0^\alpha \big|\Phi_0^\alpha\big\rangle_S, \\ \big|\Phi_0^\alpha(t)\big\rangle_S &= e^{-iE_0^\alpha t/\hbar} \big|\Phi_0^\alpha\big\rangle_S,\end{aligned} \tag{A23}$$

where the α superscript labels solutions (states and associated energy-levels), the ultimate goal is to find eigen solutions of the perturbed problem

$$\begin{aligned}\hat{H}_S \big|\Phi^\alpha\big\rangle_S &= E^\alpha \big|\Phi^\alpha\big\rangle_S, \\ \big|\Phi^\alpha(t)\big\rangle_S &= e^{-iE^\alpha t/\hbar} \big|\Phi^\alpha\big\rangle_S.\end{aligned} \tag{A24}$$

Gell-Mann and Low provided a closed form of the perturbed eigen solutions $\big(E^\alpha, |\Phi^\alpha\rangle_S\big)$ in terms of the unperturbed ones $\big(E_0^\alpha, |\Phi_0^\alpha\rangle_S\big)$ and the time-evolution operator;[154] see also Refs. 155 (pp. 61–64) and 59 (Sec. 11f). A few years later, Sucher[156] provided an expression of the perturbation energy-shift that is more symmetric in time,

$$\begin{aligned}\Delta E^\alpha &= E^\alpha - E_0^\alpha \\ &= \lim_{\substack{\epsilon\to 0 \\ \lambda\to 1}} \frac{i\epsilon\lambda}{2} \frac{\partial}{\partial\lambda} \log\big\langle \Phi_0^\alpha \big| \hat{\mathcal{S}}(\epsilon,\lambda) \big| \Phi_0^\alpha \big\rangle,\end{aligned} \tag{A25}$$

where ϵ is an energy parameter, to be shortly discussed. This energy-shift expression contains the $\mathcal{S}$-matrix operator that is defined to be the time-evolution operator that takes the interaction state from the very past, $t = -\infty$, to the very future, $t = +\infty$, and it can be written as [see Dyson in Ref. 157, Eq. (4)]

$$\hat{\mathcal{S}}(\epsilon,\lambda) = \mathrm{T}\Big[\exp\Big(\frac{\lambda}{i\hbar c} \int d^4x e^{-\frac{\epsilon}{\hbar}|t|} \hat{\mathcal{H}}_I(x) \Big) \Big]. \tag{A26}$$

In this expression, T stands for time-ordering, i.e., it reorders the inside operators such that those associated with earlier times act first. In the simplest case of two operators, the time-ordering operation is defined to be

$$\begin{aligned}\mathrm{T}\big[\hat{A}(x_1)\hat{B}(x_2)\big] &\equiv \Theta(t_1 - t_2)\hat{A}(x_1)\hat{B}(x_2) \\ &\quad \pm \Theta(t_2 - t_1)\hat{B}(x_2)\hat{A}(x_1),\end{aligned} \tag{A27}$$

where the minus sign applies when both operators $\hat{A}$ and $\hat{B}$ are of fermionic nature. Furthermore, the $\mathcal{S}$-matrix in Eq. (A26) is a functional of the interaction-Hamiltonian density $\hat{\mathcal{H}}_I(x)$ related to the interaction Hamiltonian $\hat{H}_I^1(t)$ by the following integral:

$$\hat{H}_I^1(t) = \int d^3x \hat{\mathcal{H}}_I(x). \tag{A28}$$

Recall that $\hat{H}_I^1(t)$ is the interaction-picture version of the Schrödinger-picture interaction-Hamiltonian $\hat{H}_S^1$ of Eq. (A19).

We shall note that the interaction density is multiplied by a damping factor $e^{-\frac{\epsilon}{\hbar}|t|}$, cf. Eq. (A26), where ϵ is a small positive quantity that has energy dimensions. This term is known as the "adiabatic switch" that allows the interpolation between the perturbed and unperturbed problems ($t = 0, \pm\infty$), and it was first introduced by Gell-Mann and Low in Ref. 154 (Appendix) while extending the $\mathcal{S}$-matrix formalism to cover the bound-electron problem [see also Ref. 158 (Sec. 1.3)]. The scattering matrix of Eq. (A26) may be expanded in powers of the perturbation parameter λ as

$$\begin{aligned}\hat{\mathcal{S}}(\epsilon,\lambda) &= \sum_{n=0}^{\infty} \hat{\mathcal{S}}^{(n)}(\epsilon,\lambda), \\ \hat{\mathcal{S}}^{(n)}(\epsilon,\lambda) &= \frac{1}{n!}\Big(\frac{\lambda}{i\hbar c}\Big)^n \int d^4x_1 \ldots \\ &\quad \times \int d^4x_n e^{-\frac{\epsilon}{\hbar}(|t_1|+\cdots+|t_n|)} \mathrm{T}\big[\hat{\mathcal{H}}_I(x_1)\ldots\hat{\mathcal{H}}_I(x_n)\big].\end{aligned} \tag{A29}$$

This form of the $\hat{\mathcal{S}}$-matrix expansion is known as the Dyson series, and it originated from the works of Dyson[157,159] and Schwinger.[160] Detailed derivations of the time-evolution and

$\hat{\mathcal{S}}$-matrix operators can be found in the works of Fetter and Walecka,[155] (pp. 54–58), Mandl and Shaw,[78] (Sec. 6.2), as well as Bjorken and Drell[161] (Sec. 17.2). In QED, the (perturbation) interaction-Hamiltonian density is given by

$$\hat{\mathcal{H}}_I(x) = \hat{J}_\mu(x)\hat{A}^\mu(x),$$

with

$$\hat{J}_\mu(x) = -ec\hat{\bar{\Psi}}(x)\gamma_\mu\hat{\Psi}(x), \tag{A30}$$

which explicitly couples the quantized electron-current field operator $\hat{J}_\mu$ to the photon field operator $\hat{A}^\mu$. Some authors, starting with Schwinger in Ref. 160 [Eq. (1.14)], use the symmetrized form

$$\hat{J}_\mu(x) = -\frac{ec}{2}[\hat{\bar{\Psi}}_\alpha(x), \hat{\Psi}_\beta(x)][\gamma_\mu]_{\alpha\beta} \tag{A31}$$

for the electron-current field operator, but the two forms are equivalent under time-ordering [see Eq. (29) of Ref. 162]. We recall that the electron and photon field operators are given in Eqs. (A7) and (A9), respectively. We note that the Dirac field operator with a bar on the top represents the Dirac adjoint field: $\hat{\bar{\Psi}}(x) = \hat{\Psi}^\dagger(x)\gamma^0$. At this point, the reader can see, from the last two equations, that the QED theory treats the electron-photon field (interaction) coupling perturbatively in powers of the elementary charge e.

We next consider how to expand the time-ordered product of the $\hat{\mathcal{S}}$-matrix and assign each of the obtained normal-ordered terms to a specific Feynman diagram.

4. Wick's theorem, field contractions, and propagators

Wick's theorem[62] allows writing the time-ordered products of Eq. (A29) in terms of normal-ordered products of all possible contractions, as given in the following equation:

$$\begin{aligned}\mathrm{T}\left[\hat{O}(x_1)\hat{O}(x_2)\hat{O}(x_3)\hat{O}(x_4)\ldots\right] =& :\hat{O}(x_1)\hat{O}(x_2)\hat{O}(x_3)\hat{O}(x_4)\ldots: \\ &+ :\overbrace{\hat{O}(x_1)\hat{O}(x_2)}\hat{O}(x_3)\hat{O}(x_4)\ldots: + \cdots \\ &+ :\overbrace{\hat{O}(x_1)\hat{O}(x_2)}\overbrace{\hat{O}(x_3)\hat{O}(x_4)}\ldots: + \cdots.\end{aligned} \tag{A32}$$

Contracted operators are moved next to each other, noting that under normal-ordering (fermionic), bosonic operators can be permuted as if they (anti)commuted. A contraction is represented by a line that links two operators and is defined to be the vacuum expectation value of the time-ordered product given by

$$\overbrace{\hat{O}(x_1)\hat{O}(x_2)} \equiv \langle 0|\mathrm{T}\left[\hat{O}(x_1)\hat{O}(x_2)\right]|0\rangle. \tag{A33}$$

Since our QED interaction-Hamiltonian density contains electron and photon operators, the time-ordered product in our $\mathcal{S}$-matrix of Eq. (A29) will be expanded with two types of contractions: electronic and photonic. The contraction of two electron field operators [of Eq. (A7)] components α and β is defined with respect to the last formula by

$$\begin{aligned}\overbrace{\hat{\Psi}_\alpha(x_1)\hat{\bar{\Psi}}_\beta(x_2)} &\equiv \langle 0_e|\mathrm{T}\left[\hat{\Psi}_\alpha(x_1)\hat{\bar{\Psi}}_\beta(x_2)\right]|0_e\rangle \\ &= i\hbar\left[S^F_{A^e}(x_1,x_2)\right]_{\alpha\beta},\end{aligned} \tag{A34}$$

where $\left[S^F_{A^e}(x,y)\right]_{\alpha\beta}$ is the α,β matrix component of the Feynman electron propagator, which in turn satisfies the Dirac propagator equation

$$\left[\gamma^\mu\left(i\hbar\partial_\mu + eA^e_\mu(\boldsymbol{x})\right) - m_ec\right]S^F_{A^e}(x,y) = \mathbb{1}_4\delta(x-y), \tag{A35}$$

cf. Eq. (A4). Furthermore, one can show that the following identities hold:

$$\begin{aligned}\overbrace{\hat{\bar{\Psi}}_\beta(x_2)\hat{\Psi}_\alpha(x_1)} &= -\overbrace{\hat{\Psi}_\alpha(x_1)\hat{\bar{\Psi}}_\beta(x_2)}, \\ \overbrace{\hat{\Psi}_\alpha(x_1)\hat{\Psi}_\beta(x_2)} &= \overbrace{\hat{\bar{\Psi}}_\alpha(x_1)\hat{\bar{\Psi}}_\beta(x_2)} = 0.\end{aligned} \tag{A36}$$

These relations show that the only nonzero contractions are between electron field operators and their adjoints. The free Feynman electron propagator $S^F_0(x,y)$, corresponding to the case $A_\mu(\boldsymbol{x}) = 0$, can be written as

$$S^F_0(y,x) = \lim_{\epsilon\to 0}\int \frac{d^4p}{(2\pi\hbar)^4}e^{-\frac{i}{\hbar}p\cdot(y-x)}S^F_0(p),$$

with

$$S^F_0(p) = \frac{\gamma^\mu p_\mu + m_ec}{p^2 - m_e{}^2c^2 + i\epsilon}, \tag{A37}$$

where $S^F_0(p)$ is the Fourier transformed free-electron propagator. The role of the small positive number ϵ is to shift energy-poles (at the energy–momentum relation) with respect to the Feynman prescription.

Similarly, the contraction of two photon operators [of Eq. (A9)] is defined by the following expression:

$$\begin{aligned}\overbrace{\hat{A}_\mu(x_1)\hat{A}_\nu(x_2)} &\equiv \langle 0_p|\mathrm{T}\left[\hat{A}_\mu(x_1)\hat{A}_\nu(x_2)\right]|0_p\rangle \\ &= i\hbar D^F_{\mu\nu}(x_1,x_2),\end{aligned} \tag{A38}$$

where $D^F_{\mu\nu}(x,y)$, the photon propagator in the Feynman gauge, is given by the expression

$$D^F_{\mu\nu}(x,y) = \lim_{\epsilon\to 0}\int \frac{d^4p}{(2\pi\hbar)^4}e^{-\frac{i}{\hbar}p\cdot(x-y)}D^F_{\mu\nu}(p),$$

with

$$D^F_{\mu\nu}(p) = g_{\mu\nu}D^F(p) = -\frac{\hbar^2}{c\epsilon_0}\frac{g_{\mu\nu}}{p^2 + i\epsilon}, \tag{A39}$$

and it satisfies the Maxwell Green's-type equation

$$\partial_\sigma\partial^\sigma D^F_{\nu\theta}(x,y) = \frac{g_{\nu\theta}}{\epsilon_0 c}\delta(x-y). \tag{A40}$$

This equation is obtained after imposing the Lorenz gauge condition, otherwise this propagator will not be invertible; see Schwartz

in Ref. 163 (Sec. 8.5). We should finally note that the F superscript on both propagators is added to indicate that these are Feynman propagators. This means that when writing the propagators as Fourier transforms, the energy-integrals are to be taken along the Feynman contour. Different choices of paths (contours) lead to different propagators (retarded and advanced), but they all satisfy the corresponding Dirac and Maxwell equations.

5. Bound-electron propagator expansion

The bound Feynman propagator $S^F_{A^e}(x_2,x_1)$ of Eq. (A34) can be expanded in powers of the external potential as [Refs. 86, Eqs. (2)–(119) and 164, Eq. (16)]

$$S^F_{A^e}(x_2,x_1) = S^F_0(x_2,x_1) - \int d^4x_3 S^F_0(x_2,x_3) e A^e_\mu(\boldsymbol{x}_3)\gamma^\mu S^F_0(x_3,x_1) + \cdots \tag{A41}$$

and written in terms of the free-electron propagator $S^F_0(x_2,x_1)$ of Eq. (A37). It is worth noting that the bound Feynman propagator can be related to the bound Dirac Green's function G_{A^e} by the relation of Ref. 162 [Eq. (32)]

$$S^F_{A^e}(x_2,x_1) = \frac{1}{i\hbar}\frac{1}{2\pi i}\int_{C_F} dz\; G_{A^e}(\boldsymbol{x}_2,\boldsymbol{x}_1;z)\gamma^0 e^{-\frac{i}{\hbar}z(t_2-t_1)}. \tag{A42}$$

This Green's function satisfies

$$[H_D(\boldsymbol{x}_2) - z]G_{A^e}(\boldsymbol{x}_2,\boldsymbol{x}_1;z) = \mathbb{1}_4\delta(\boldsymbol{x}_2-\boldsymbol{x}_1), \tag{A43}$$

cf. Eqs. (A4) and (A35). Using Eqs. (A41) and (A42), and integrating over time variables, one obtains the potential expansion associated with the Green's function given by

$$G_{A^e}(\boldsymbol{x}_2,\boldsymbol{x}_1;z) = G_0(\boldsymbol{x}_2,\boldsymbol{x}_1;z) + ec\int d^3x_3 G_0(\boldsymbol{x}_2,\boldsymbol{x}_3;z) \times A^e_\mu(\boldsymbol{x}_3)\alpha^\mu G_0(\boldsymbol{x}_3,\boldsymbol{x}_1;z) + \cdots, \tag{A44}$$

where the free Dirac Green's function is given by $G_0 = \lim_{A^e\to 0} G_{A^e}$. These two expansions are known as the potential expansion, where consecutive terms are known as the zero-, one-, and many-potential terms. The main utility of this expansion is that it allows the isolation of ultraviolet divergent integrals encountered when evaluating loop integrals as done by Baranger *et al.*,[72] and later by many authors working within the BSQED theory.

6. No-photon BSQED energy-shifts

Using the $\mathcal{S}$-matrix expansion of Eq. (A29), one can expand Sucher's energy-shift expression of Eq. (A25) in powers of the interaction-Hamiltonian density and write, following Mohr in Ref. 165 [Eqs. (18) and (31)],

$$\Delta E^\alpha = \lim_{\substack{\epsilon\to 0\\ \lambda\to 1}} \frac{i\epsilon\lambda}{2}\Big[\Big\langle\Phi^\alpha_0\Big|\hat{\mathcal{S}}^{(1)}(\epsilon,\lambda)\Big|\Phi^\alpha_0\Big\rangle + 2\Big\langle\Phi^\alpha_0\Big|\hat{\mathcal{S}}^{(2)}(\epsilon,\lambda)\Big|\Phi^\alpha_0\Big\rangle - \Big\langle\Phi^\alpha_0\Big|\hat{\mathcal{S}}^{(1)}(\epsilon,\lambda)\Big|\Phi^\alpha_0\Big\rangle^2 + \mathcal{O}(\lambda^3)\Big], \tag{A45}$$

where $\hat{\mathcal{S}}^{(n)}$ is given in Eq. (A29). We shall now consider a system of n electrons and zero photons (photon vacuum), represented by the following electron-photon state, labeled by α:

$$\big|\Phi^\alpha_0\big\rangle = \big|n^\alpha_e, 0^\alpha_p\big\rangle. \tag{A46}$$

We remind the reader that the electron field operators entering in our expressions describe noninteracting electrons, in the presence of an external potential, as also seen in the zeroth-order electron Hamiltonian of Eq. (A21). As already pointed out in Sec. II, the electron–electron interaction arises from terms describing exchange of virtual photons between bound electrons.

Since the photon state is chosen to be the vacuum one, this means that any string of photon operators that is not fully contracted will vanish under the photon vacuum expectation value of Eq. (A25). Following this reasoning, one concludes that the first non-vanishing QED correction comes from the second-order $\hat{\mathcal{S}}^{(2)}$-matrix

$$\hat{\mathcal{S}}^{(2)}(\epsilon,\lambda) = -\frac{\lambda^2}{2\hbar^2c^2}\int d^4x_1\int d^4x_2\; e^{-\frac{\epsilon}{\hbar}(|t_1|+|t_2|)}\mathrm{T}\big[\hat{\mathcal{H}}_I(x_1)\hat{\mathcal{H}}_I(x_2)\big]. \tag{A47}$$

Using Wick's theorem, we expand the electron and photon time-ordered products and then replace operator contractions by their corresponding propagators, following the contraction definitions of Eqs. (A34) and (A38). Furthermore, using the symmetry properties of the photon propagator of Eq. (A39),

$$D^F_{\mu\nu}(x,y) = D^F_{\mu\nu}(y,x) = D^F_{\nu\mu}(x,y), \tag{A48}$$

the second-order $\mathcal{S}$-matrix of Eq. (A47) can be shown to reduce to the following expression:

$$\hat{\mathcal{S}}^{(2)}(\epsilon,\lambda) = -\frac{\lambda^2e^2}{2\hbar^2}\int d^4x_1\int d^4x_2 e^{-\frac{\epsilon}{\hbar}(|t_1|+|t_2|)}\hat{F}(x_1,x_2), \tag{A49}$$

where the operator $\hat{F}(x_1,x_2)$ contains the following five QED corrections to the noninteracting problem:

$$\begin{aligned}
\hat{F}(x_1,x_2) = {} & i\hbar\; D^F_{\mu_1\mu_2}(x_1,x_2) : \hat{\bar{\Psi}}(x_1)\gamma^{\mu_1}\hat{\Psi}(x_1)\hat{\bar{\Psi}}(x_2)\gamma^{\mu_2}\hat{\Psi}(x_2) : && \text{SP}\\
& + 2\hbar^2 D^F_{\mu_1\mu_2}(x_1,x_2)\,\mathrm{Tr}\big[S^F_{A^e}(x_2,x_2)\gamma^{\mu_2}\big] : \hat{\bar{\Psi}}(x_1)\gamma^{\mu_1}\hat{\Psi}(x_1) : && \text{VP}\\
& - 2\hbar^2 D^F_{\mu_1\mu_2}(x_1,x_2) : \hat{\bar{\Psi}}(x_1)\gamma^{\mu_1}S^F_{A^e}(x_1,x_2)\gamma^{\mu_2}\hat{\Psi}(x_2) : && \text{SE}\\
& - i\hbar^3 D^F_{\mu_1\mu_2}(x_1,x_2)\,\mathrm{Tr}\big[S^F_{A^e}(x_1,x_1)\gamma^{\mu_1}\big]\,\mathrm{Tr}\big[S^F_{A^e}(x_2,x_2)\gamma^{\mu_2}\big] && \text{D1}\\
& + i\hbar^3 D^F_{\mu_1\mu_2}(x_1,x_2)\,\mathrm{Tr}\big[S^F_{A^e}(x_2,x_1)\gamma^{\mu_1}S^F_{A^e}(x_1,x_2)\gamma^{\mu_2}\big] && \text{D2.}
\end{aligned} \tag{A50}$$

Finally, using Sucher's energy expression of Eq. (A45), the second-order energy-shift becomes

$$\Delta E^{\alpha,2} = \lim_{\substack{\epsilon\to 0\\ \lambda\to 1}} i\epsilon\lambda\left\langle\Phi_0^\alpha\middle|\hat{\mathcal{S}}^{(2)}(\epsilon,\lambda)\middle|\Phi_0^\alpha\right\rangle = \Delta E^{\alpha,2}_{\mathrm{SP}} + \Delta E^{\alpha,2}_{\mathrm{VP}} + \Delta E^{\alpha,2}_{\mathrm{SE}} + \Delta E^{\alpha,2}_{\mathrm{D1}} + \Delta E^{\alpha,2}_{\mathrm{D2}}. \tag{A51}$$

Each of these terms will be discussed in the next sections and is represented by a Feynman diagram in Fig. 1. The elements of these diagrams are the following:

1. Double external lines represent bound electrons, i.e., with wavefunctions and energies satisfying the interacting Dirac equation of Eq. (A4), in the presence of a classical time-independent external potential $A^e(\boldsymbol{x})$.
2. Double internal lines represent a virtual bound-electron propagation between the two vertices $S^F_{A^e}(x_2,x_1)$ and arise from a single contraction of two electron field operators.
3. Internal wiggly lines connecting two vertices represent propagations of virtual-photons $D^F_{\mu_2\mu_1}(x_2,x_1)$ and come from a single contraction of two photon field operators.

The last two contributions from Eq. (A50) correspond to fully contracted products, and they are thus free of creation and annihilation operators. This means that their corresponding energy-shifts $\Delta E^{\alpha,2}_{\mathrm{D1}}$ and $\Delta E^{\alpha,2}_{\mathrm{D2}}$ are state-independent and hence do not contribute to energy-differences. They are therefore discarded from further consideration; see for instance Mohr in Ref. 165. On the other hand, the first three contributions correspond to partially contracted products, associated with the following physical processes:

a. SP: Single-photon exchange

This process, coming from the SP term in Eq. (A50) and represented in Fig. 1(a), describes electron–electron interaction in its lowest order, where an electron feels the existence of the other electron through the exchange of a single virtual-photon. After integrating over times t_1 and t_2 in Eq. (A49), and taking limits in Eq. (A51), this correction yields an instantaneous direct interaction-term, in addition to a retarded exchange interaction-term, analogous to the direct and exchange terms in the Hartree–Fock theory,

$$\begin{aligned}\Delta E^{\alpha,2}_{\mathrm{SP}} = {}& \frac{e^2}{2}\sum_{i,j}\int d^3x_1\int d^3x_2\,\bar\psi_i(\boldsymbol{x}_1)\gamma^\mu\psi_i(\boldsymbol{x}_1)\\ &\times\frac{1}{4\pi\epsilon_0|\boldsymbol{x}_1-\boldsymbol{x}_2|}\bar\psi_j(\boldsymbol{x}_2)\gamma_\mu\psi_j(\boldsymbol{x}_2)\quad\text{Direct}\\ &-\frac{e^2}{2}\sum_{i,j}\int d^3x_1\int d^3x_2\,\bar\psi_i(\boldsymbol{x}_1)\gamma^\mu\psi_j(\boldsymbol{x}_1)\\ &\times\frac{e^{+\frac{i}{c\hbar}|E_i-E_j||\boldsymbol{x}_1-\boldsymbol{x}_2|}}{4\pi\epsilon_0|\boldsymbol{x}_1-\boldsymbol{x}_2|}\bar\psi_j(\boldsymbol{x}_2)\gamma_\mu\psi_i(\boldsymbol{x}_2)\quad\text{Exchange},\end{aligned} \tag{A52}$$

as noted by Mohr in Ref. 166 (Sec. IV). Notice that for $\mu=0$ and $\mu=1,2,3$, these integrals account for the Coulomb and Gaunt interaction, respectively. On the other hand, if we used the Coulomb gauge photon propagator instead of the Feynman one, we would get the retarded Breit interaction, as noted by Lindgren in Ref. 167 (p. 262).

b. VP: Vacuum polarization

This process, presented in Fig. 1(b), accounts for the instantaneous interaction of a bound electron with the electron–positron pair cloud polarized by the presence of a classical potential source. After plugging the VP term of Eq. (A50) in the second-order scattering matrix expression, one can use Sucher's formula of Eq. (A45) to write the energy-shift associated with the vacuum polarization process as Ref. 59 [Chap. 15, Eq. (205)],

$$\Delta E^{\alpha}_{\mathrm{VP}} = -e\sum_i\int d^3x_1\,\bar\psi_i(\boldsymbol{x}_1)\gamma_\mu\psi_i(\boldsymbol{x}_1)\varphi^\mu_{\mathrm{VP}}(\boldsymbol{x}_1). \tag{A53}$$

We note that the vacuum polarization effect is local, i.e., it can be written as an expectation value of a local vacuum polarization four-potential given by

$$\varphi^\mu_{\mathrm{VP}}(\boldsymbol{x}_1) = ie\hbar\int d^3x_2\,\frac{\mathrm{Tr}\left[\gamma^\mu S^F_{A^e}(x_2,x_2)\right]}{4\pi\epsilon_0|\boldsymbol{x}_1-\boldsymbol{x}_2|}. \tag{A54}$$

The energy expression of Eq. (A53) (as well as the last potential) is divergent due to the fact that

$$\lim_{x_1\to x_2} S^F_{A^e}(x_2,x_1) = \infty, \tag{A55}$$

as mentioned in Ref. 168. The isolation of the divergent terms in this expression can be done by expanding the propagator inside the trace using Eq. (A41), and the energy can be written as

$$\Delta E^{\alpha,2}_{\mathrm{VP}} = \Delta E^{\alpha,2}_{\mathrm{VP},0} + \Delta E^{\alpha,2}_{\mathrm{VP},1} + \Delta E^{\alpha,2}_{\mathrm{VP},2} + \cdots \tag{A56}$$

where $\Delta E^{\alpha,2}_{\mathrm{VP},i}$ represents the term that corresponds to an i number of interactions with the external potential $(Z\alpha)^i$. The first four terms are presented in Figs. 3(a)–3(d). Notice that the double-line loop is replaced by a single-line one. This is made to indicate that the propagators between these vertices are the free ones S^F_0 instead of the bound ones $S^F_{A^e}$. Using Furry's theorem,[169] which is based on a charge conjugation symmetry argument, one can show that diagrams containing a free-electron loop with an odd number of vertices do not contribute. This means that the above energy expression reduces to

$$\Delta E^{\alpha,2}_{\mathrm{VP}} = \Delta E^{\alpha,2}_{\mathrm{VP},1} + \Delta E^{\alpha,2}_{\mathrm{VP},3} + \cdots \tag{A57}$$

A naive estimation of the degree of divergence of a QED integral can be done by calculating the superficial degree of divergence S that simply counts overall momentum powers of the integral in question (in momentum-space),

$$S \equiv 4 - N_e - 2N_p, \tag{A58}$$

where four is the spacetime dimension and N_e and N_p are the number of electron and photon propagators, respectively, in the loop in question; see for instance Refs. 60 (Sec. 10.1) and 86 (Secs. 7-1-4 and 8-1-3). The integral is said to be superficially divergent if $S\geq 0$. The possible cases are

$$\begin{aligned} S\leq 0:&\quad\text{convergence},\\ S=0:&\quad\text{logarithmic divergence},\\ S=1:&\quad\text{linear divergence},\\ S=2:&\quad\text{quadratic divergence}.\end{aligned} \tag{A59}$$

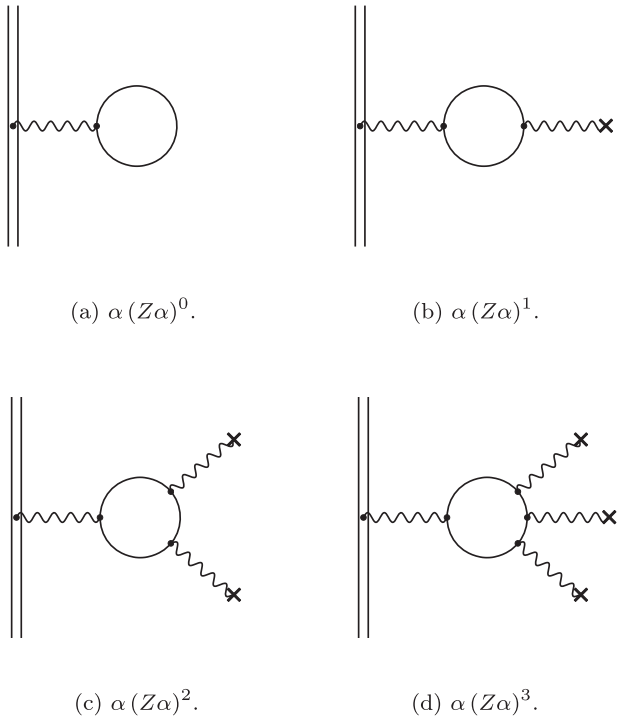

FIG. 3. First four bound-state vacuum polarization processes, obtained after expanding the bound propagator in powers of the external potential. A wiggly line ending with a cross × indicates an interaction with the external field. (a) $\alpha(Z\alpha)^0$, (b) $\alpha(Z\alpha)^1$, (c) $\alpha(Z\alpha)^2$, and (d) $\alpha(Z\alpha)^3$.

This naive estimation usually overestimates the effective degree of divergence, which we shall call E, and this can be seen after further analysis of the integral in question. As a consequence, some superficially divergent integrals can be effectively less divergent, or hopefully convergent. In Table XVII, we list the superficial and effective divergences of the first vacuum polarization terms. The reader should notice that with higher-order terms, more propagators are included in the momentum-space integral, meaning that more denominator powers are added, and as a consequence, the integral becomes less divergent.

We shall now focus on the first non-vanishing vacuum polarization contribution $\Delta E^{\alpha}_{\mathrm{VP},1}$. As seen in Table XVII, this term is of superficial quadratic divergence, but it is effectively only logarithmic. This can be shown using the Ward identity, as mentioned by Peskin and Schroeder in Ref. 60 (Sec. 7.5). After the employment of regularization, followed by renormalization (discussed in Subsection 6 d of the Appendix), one may extract the physical contribution out of the divergent $\Delta E^{\alpha,2}_{\mathrm{VP},1}$. In the case where the Hamiltonian is invariant under time-reversal symmetry, i.e., if the external vector potential $\boldsymbol{A}^e(\boldsymbol{x})$ vanishes, cf. Greiner in Ref. 170 [Eqs. (12.52) and (12.53)], then only the time-component potential $\varphi^0_{\mathrm{VP},1}$ survives, and one obtains the Uehling potential,[23] given in Eq. (8).

TABLE XVII. Superficial and effective degrees of divergence for the bound-state vacuum polarization contributions.

Terms	S	E
$\alpha(Z\alpha)^1$	2	0
$\alpha(Z\alpha)^3$	0	<0
$\alpha(Z\alpha)^5$	<0	<0
...	...	...

For detailed discussions and derivations of the one-potential bound-state vacuum polarization correction, the reader may consult the calculation of Greiner and Reinhardt in Ref. 85 (Sec. 5.2) where the authors used Pauli–Villars regularization in addition to that of Peskin and Schroeder in Ref. 60 (Sec. 7.5) who used dimensional regularization to treat the occurring divergences; see also the work of Mandl and Shaw in Ref. 78 (Sec. 10.4), in addition to Schwartz in Ref. 163 (Sec. 16.2.2). Contrary to the conventional momentum-space approach to evaluate QED corrections, Indelicato and Mohr in Ref. 168 (Sec. B) considered the vacuum polarization problem in coordinate-space and derived the physical Uehling contribution using coordinate-space Pauli–Villars regularization.

The second non-vanishing vacuum polarization effect, associated with $\Delta E^{\alpha,2}_{\mathrm{VP},3}$ and presented in Fig. 3(d), is known as the Wichmann–Kroll effect.[70] As seen in Table XVII and noted by Gyulassy,[171] this contribution is free of divergences. Wichmann and Kroll calculated the effective potential associated with the $\Delta E^{\alpha,2}_{\mathrm{VP},3}$ correction in Laplace space. On the other hand, in Ref. 172 (Sec. 4), Blomqvist has evaluated the inverse Laplace-transform and obtained the real-space potential expression for a point nuclear charge distribution. The last reference presents a relatively complex analytical expression for this $\alpha(Z\alpha)^3$ potential, and this motivated Fainshtein *et al.*[173] to provide an approximation that facilitates the numerical computation while conserving precision.

We finally note that in the fourth-order BSQED correction, one finds the Källén–Sabry potentials[71] of order $\alpha^2(Z\alpha)$ that can be obtained by expanding the bound propagators of Ref. 162 [Fig. 25 diagrams (b) and (c) VPVP]. In order to make this momentum-space potential useable in practical calculations, in Ref. 172 (Sec. 3), Blomqvist derived its real-space version for a point nucleus distribution, whereas Fullerton and Rinker generalized this result to account for an extended nuclear charge distribution; see Ref. 66 [Eq. (9)]. We finally note that the latter authors provided a good approximation of the corresponding potential in order to render the numerical evaluation more practical.

c. SE: Self-energy

The self-energy process, presented in Fig. 1(c), is the dominant radiative QED correction in electronic atoms, as seen in the work of Johnson and Soff of Ref. 123 (Fig. 2). This process describes the interaction of the bound electron with itself by emitting and absorbing a virtual-photon. The first calculation for this correction was made in 1947 by Bethe in a purely nonrelativistic framework,[174] where he used a renormalization technique (by subtracting the free self-energy) to render the integral less divergent and introduced a reasonable virtual-photon energy cutoff at $E = m_e c^2$. This simple calculation gave hope in digging for the physical Lamb shift in the frustrating nonphysical divergences in the QED theory. Using Sucher's energy formula of Eq. (A45), the SE term of Eq. (A50) leads to the following energy-shift:

$$\Delta E_{\rm SE}^{\alpha,2} = -e\sum_i \int d^3x_1 \int d^3x_2 \psi_i^\dagger(\boldsymbol{x}_2)\varphi_{\rm SE}(\boldsymbol{x}_2,\boldsymbol{x}_1;E_i)\psi_i(\boldsymbol{x}_1), \quad \text{(A60)}$$

where the self-energy potential is given by

$$\varphi_{\rm SE}(\boldsymbol{x}_2,\boldsymbol{x}_1;E_i) = -\frac{e}{2\pi i}\int_{C_F} dz\alpha^\mu G_{A^e}(\boldsymbol{x}_2,\boldsymbol{x}_1;z)\alpha_\mu \times \frac{\exp\left(+\frac{i}{\hbar}|\boldsymbol{x}_1-\boldsymbol{x}_2|\sqrt{(z-E_i)^2/c^2+i\epsilon}\right)}{4\pi\epsilon_0|\boldsymbol{x}_1-\boldsymbol{x}_2|}. \quad \text{(A61)}$$

Similar forms of this equation are provided by Schweber in Ref. 59 [Eq. (205)] and Mohr in Ref. 175 [Eq. (2.6)]. Notice at this point that unlike the vacuum polarization case, the self-energy is a nonlocal effect, as seen from Eq. (A60), and this is the reason behind the complexity of its analytical and numerical evaluation. As in the vacuum polarization case, the self-energy potential is a divergent quantity and needs to be regularized. In order to isolate divergent terms, one can use the Green's function (propagator) expansion of Eq. (A44) and write the total energy-shift as

$$\Delta E_{\rm SE}^{\alpha,2} = \Delta E_{\rm SE,0}^{\alpha,2} + \Delta E_{\rm SE,1}^{\alpha,2} + \Delta E_{\rm SE,2}^{\alpha,2} + \cdots, \quad \text{(A62)}$$

where $\Delta E_{{\rm SE},i}^{\alpha,2}$ represents the process in which the internal electron interacts i times with the external potential, it is thus associated with the $\alpha(Z\alpha)^i$ order. The first four terms of the last expansion are represented in Figs. 4(a)–4(d). The zero- and one-potential terms, $\Delta E_{\rm SE,0}^{\alpha,2}$ and $\Delta E_{\rm SE,1}^{\alpha,2}$, are known as the (free) self-energy and the vertex-correction processes. These two contributions are logarithmically divergent (in momentum-space), while all higher-order ones are convergent, as presented in Table XVIII. A coordinate-space treatment of these quantities has been provided by Indelicato and Mohr.[75,168,175] Using the bound propagator expansion of Eq. (A41), one obtains the scattering matrices associated with these two processes:

$$\hat{\mathcal{S}}_{\rm SE,0}^{(2)}(\epsilon,\lambda) = \lambda^2 e^2 \int d^4x_1 \int d^4x_2 e^{-\frac{\epsilon}{\hbar}(|t_1|+|t_2|)} D_{\mu_1\mu_2}^F(x_1,x_2) : \times \bar{\hat{\Psi}}(x_1)\gamma^{\mu_2} S_0^F(x_1,x_2)\gamma^{\mu_1}\hat{\Psi}(x_2) :, \quad \text{(A63)}$$

$$\hat{\mathcal{S}}_{\rm SE,1}^{(2)}(\epsilon,\lambda) = -\lambda^2 e^2 \int d^4x_1 \int d^4x_2 e^{-\frac{\epsilon}{\hbar}(|t_1|+|t_2|)} D_{\mu_1\mu_2}^F(x_1,x_2) : \times \bar{\hat{\Psi}}(x_1)\gamma^{\mu_1} \int d^4x_3 S_0^F(x_1,x_3) e A_\mu^e(\boldsymbol{x}_3) \times \gamma^\mu S_0^F(x_3,x_2)\gamma^{\mu_2}\hat{\Psi}(x_2) :. \quad \text{(A64)}$$

The next step is to transform these two real-space integral $\mathcal{S}$-matrices into Fourier-space ones. We first use the electron and photon propagators of Eqs. (A37) and (A39) and write electron field operators and the external (classical) potential in their Fourier-integral forms,

$$\hat{\Psi}(x) = \int \frac{d^4p}{(2\pi\hbar)^4} e^{-\frac{i}{\hbar}p\cdot x}\hat{\Psi}(p), \qquad A^e(x) = \int \frac{d^4p}{(2\pi\hbar)^4} e^{-\frac{i}{\hbar}p\cdot x} A^e(p). \quad \text{(A65)}$$

We finally note that variable dependence indicates in which space the corresponding physical quantity is: We use x variables for space-time points (coordinate-space) and p and q variables for four-momentum points (in momentum-space). The first $\mathcal{S}$-matrix $\hat{\mathcal{S}}_{\rm SE,0}^{(2)}(\epsilon,\lambda)$ (the zero-potential bound-state self-energy) becomes

$$\hat{\mathcal{S}}_{\rm SE,0}^{(2)}(0,1) = \int \frac{d^4q}{(2\pi\hbar)^4} : \bar{\hat{\Psi}}(q)\gamma^\mu\Sigma(q)\gamma_\mu\hat{\Psi}(q) :, \quad \text{(A66)}$$

$$\Sigma(q) = e^2 \int \frac{d^4p}{(2\pi\hbar)^4} S_0^F(q-p)D^F(p). \quad \text{(A67)}$$

Here, $\Sigma(q)$ is the so-called self-energy matrix function {see, for instance, Mandl and Shaw in Ref. 78 [Eq. (9.20)]}. Notice that in the limit of large momentum p, the integrand behaves as $\propto \frac{1}{\gamma^\mu(q-p)_\mu}\frac{1}{p^3}$,

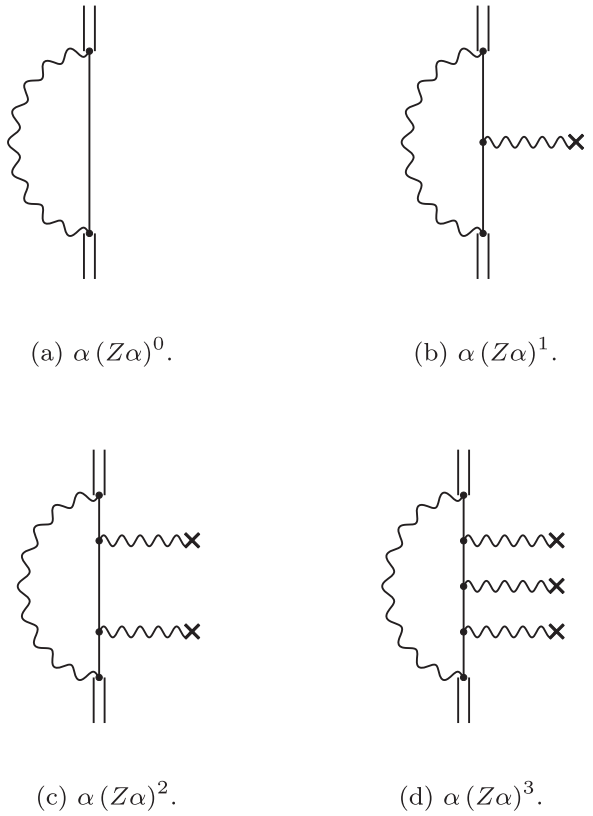

(a) $\alpha(Z\alpha)^0$. (b) $\alpha(Z\alpha)^1$. (c) $\alpha(Z\alpha)^2$. (d) $\alpha(Z\alpha)^3$.

FIG. 4. First four bound-state self-energy processes, obtained after expanding the bound propagator in powers of the external potential. (a) $\alpha(Z\alpha)^0$, (b) $\alpha(Z\alpha)^1$, (c) $\alpha(Z\alpha)^2$, and (d) $\alpha(Z\alpha)^3$.

TABLE XVIII. Superficial and effective degrees of divergence for the bound-state self-energy contributions.

Terms	S	E
$\alpha(Z\alpha)^0$	1	0
$\alpha(Z\alpha)^1$	0	0
$\alpha(Z\alpha)^2$	<0	<0
...	...	...

which indicates a superficial linear divergence. However, with further investigation, one can show that this divergence is reduced by one degree, as noted by Schweber in Ref. 59 (Sec. 15a), and presented in Table XVIII. Following the same steps, one can show that the second scattering matrix, associated with the one-potential bound-state self-energy process $\hat{\mathcal{S}}^{(2)}_{\mathrm{SE},0}(0,1)$, can be written as

$$\hat{\mathcal{S}}^{(2)}_{\mathrm{SE},1}(0,1) = -\frac{e}{i\hbar}\int \frac{d^4p_2}{(2\pi\hbar)^4}\int \frac{d^4p_1}{(2\pi\hbar)^4} A^e_\mu(p_2-p_1):, \\ \times \hat{\bar{\Psi}}(p_2)\Lambda^\mu(p_2,p_1)\hat{\Psi}(p_1):, \tag{A68}$$

$$\Lambda^\mu(p_2,p_1) = i\hbar e^2\gamma^\nu \int \frac{d^4q}{(2\pi\hbar)^4} D^F(q) S^F_0(p_2-q)\gamma^\mu S^F_0(p_1-q)\gamma_\nu, \tag{A69}$$

where in the last equation, $\Lambda^\mu(p_2,p_1)$ is the so-called vertex-correction function; see, for instance, the work by Mandl and Shaw[78] [Eq. (9.48)]. A detailed study of these momentum-space expressions and associated energy-shifts in the bound-electron problem was first considered by Snyderman in Ref. 176 (Sec. 4) (see also the work by Yerokhin and Shabaev[177]).

d. Regularization and renormalization

When computing integrals associated with QED corrections, one finds (as already seen) that some of these integrals are divergent. How can one extract the meaningful finite (physical) from the meaningless infinite? This is done through regularization and renormalization.

Regularization is a technique for rendering a divergent integral convergent, albeit still dependent on the regularization-parameter. The main regularization techniques are sharp momentum-cutoff, Pauli–Villars,[178] dimensional-regularization,[179] and analytic continuation[180] regularization. The reader may also consult the work of Zeidler in Ref. 181 (Chap. 2) for a general conceptual formulation of regularization schemes. The sharp momentum-cutoff regularization consists of cutting off momentum contributions higher than a some $p_{\max} = \Lambda \gg m_e c$. Unfortunately, this intuitive regularization breaks Lorentz- and gauge-invariance and the solution is to use the other regularization schemes. The Pauli–Villars regularization consists of modifying the photon and electron propagators by introducing new propagators, associated with auxiliary masses (entering in propagators), for the self-energy and vacuum polarization processes. Finally, one can use dimensional regularization, which is based on the fact that logarithmically divergent integrals (as for the divergences associated basic QED processes) are convergent if one modifies the space-time dimensions through $d = 4 \to d = 4 - \epsilon$, where ϵ is a small positive number. In all cases, after regularization, the divergent integrals are parameterized by the regularization parameters and are still divergent in the limit $\Lambda \to \infty$ or $\epsilon \to 0$, for instance. This is where renormalization comes into play.

Renormalization is a mathematical technique that consists of redefining the electron mass and charge (in addition to fields) such that the divergences, coming from including the QED corrections, are eliminated: absorbed by the bare physical quantities. It should be noted at this point that the experimentally observed mass and charge, m_{exp} and e_{exp}, are results of experiments that already include QED corrections. On the other hand, one can imagine a world in which the QED interaction is switched off; in this world, one would measure what is known as bare mass and charge: m_0 and e_0. This distinction clearly shows that the electron mass and charge that we start with (before switching QED on: before taking it into consideration) should be the bare ones instead of the measured ones. This awareness played a crucial role in formulating the renormalization theory. Since we do not have access to bare quantities, and since infinity is not natural (not measurable), the renormalization theory says that we are allowed to redefine our physical constants such that the bare ones absorb the emerging divergences and lead to overall values of the physical constants that correspond to the experimentally observed ones. Detailed discussions on renormalization in the quantum field theory are provided by Collins in Ref. 182, Greiner and Reinhardt in Ref. 85 (Chap. 5), Peskin and Schroeder in Ref. 60 (Chap. 7), Itzykson and Zuber in Ref. 86 (Sec. 7.1), and Huang in Refs. 183 (Chap. 13) and 184.

REFERENCES

[1] K. G. Dyall and K. Fægri, Jr., *Introduction to Relativistic Quantum Chemistry* (Oxford University Press, 2007).
[2] M. Reiher and A. Wolf, *Relativistic Quantum Chemistry: The Fundamental Theory of Molecular Science* (John Wiley & Sons, 2014).
[3] T. Saue, ChemPhysChem **12**, 3077 (2011).
[4] P. Pyykkö, Annu. Rev. Phys. Chem. **63**, 45 (2012).
[5] P. Schwerdtfeger, L. F. Pašteka, A. Punnett, and P. O. Bowman, Nucl. Phys. A **944**, 551 (2015).
[6] P. Pyykko and J. P. Desclaux, Acc. Chem. Res. **12**, 276 (1979).
[7] P. Pyykko, Chem. Rev. **88**, 563 (1988).
[8] R. Ahuja, A. Blomqvist, P. Larsson, P. Pyykkö, and P. Zaleski-Ejgierd, Phys. Rev. Lett. **106**, 018301 (2011).
[9] E. Eliav, U. Kaldor, and Y. Ishikawa, Chem. Phys. Lett. **222**, 82 (1994).
[10] N. N. Dutta and S. Majumder, Phys. Rev. A **85**, 032512 (2012).
[11] A. Shee, T. Saue, L. Visscher, and A. S. P. Gomes, J. Chem. Phys. **149**, 174113 (2018).
[12] T. Saue and L. Visscher, *Theoretical Chemistry and Physics of Heavy and Superheavy Elements* (Springer, 2003), pp. 211–267.
[13] W. Liu and I. Lindgren, J. Chem. Phys. **139**, 014108 (2013).
[14] W. E. Lamb and R. C. Retherford, Phys. Rev. **72**, 241 (1947).
[15] Th. Stöhlker, P. H. Mokler, F. Bosch, R. W. Dunford, F. Franzke, O. Klepper, C. Kozhuharov, T. Ludziejewski, F. Nolden, H. Reich *et al.*, Phys. Rev. Lett. **85**, 3109 (2000).
[16] P. Pyykkö, Chem. Rev. **112**, 371 (2012).
[17] P. Pyykkö, M. Tokman, and L. N. Labzowsky, Phys. Rev. A **57**, R689 (1998).
[18] H. Persson, I. Lindgren, and S. Salomonson, Phys. Scr. **T46**, 125 (1993).
[19] H. Persson, I. Lindgren, S. Salomonson, and P. Sunnergren, Phys. Rev. A **48**, 2772 (1993).
[20] M. Puchalski and K. Pachucki, Phys. Rev. Lett. **111**, 243001 (2013).
[21] M. Haidar, Z.-X. Zhong, V. Korobov, and J.-P. Karr, Phys. Rev. A **101**, 022501 (2020).
[22] T. Aoyama, M. Hayakawa, T. Kinoshita, and M. Nio, Phys. Rev. Lett. **109**, 111807 (2012).
[23] E. A. Uehling, Phys. Rev. **48**, 55 (1935).
[24] P. Pyykkö and L.-B. Zhao, J. Phys. B: At., Mol. Opt. Phys. **36**, 1469 (2003).
[25] V. V. Flambaum and J. S. M. Ginges, Phys. Rev. A **72**, 052115 (2005).
[26] V. M. Shabaev, I. I. Tupitsyn, and V. A. Yerokhin, Phys. Rev. A **88**, 012513 (2013).
[27] A. V. Malyshev, D. A. Glazov, V. M. Shabaev, I. I. Tupitsyn, V. A. Yerokhin, and V. A. Zaytsev, Phys. Rev. A **106**, 012806 (2022).
[28] K. G. Dyall, I. P. Grant, C. T. Johnson, F. A. Parpia, and E. P. Plummer, Comput. Phys. Commun. **55**, 425 (1989).

[29]V. M. Shabaev, I. I. Tupitsyn, and V. A. Yerokhin, Comput. Phys. Commun. **189**, 175 (2015).
[30]V. M. Shabaev, I. I. Tupitsyn, and V. A. Yerokhin, Comput. Phys. Commun. **223**, 69 (2018).
[31]E. V. Kahl and J. C. Berengut, Comput. Phys. Commun. **238**, 232 (2019).
[32]L. F. Pašteka, E. Eliav, A. Borschevsky, U. Kaldor, and P. Schwerdtfeger, Phys. Rev. Lett. **118**, 023002 (2017).
[33]B. C. Shepler, N. B. Balabanov, and K. A. Peterson, J. Phys. Chem. A **109**, 10363 (2005).
[34]B. C. Shepler, N. B. Balabanov, and K. A. Peterson, J. Chem. Phys. **127**, 164304 (2007).
[35]K. A. Peterson, J. Chem. Phys. **142**, 074105 (2015).
[36]R. M. Cox, M. Citir, P. B. Armentrout, S. R. Battey, and K. A. Peterson, J. Chem. Phys. **144**, 184309 (2016).
[37]R. Feng and K. A. Peterson, J. Chem. Phys. **147**, 084108 (2017).
[38]T. Hangele, M. Dolg, M. Hanrath, X. Cao, and P. Schwerdtfeger, J. Chem. Phys. **136**, 214105 (2012).
[39]T. Hangele, M. Dolg, and P. Schwerdtfeger, J. Chem. Phys. **138**, 174113 (2013).
[40]T. Hangele and M. Dolg, Chem. Phys. Lett. **616–617**, 222 (2014).
[41]T. Hangele and M. Dolg, J. Chem. Phys. **138**, 044104 (2013).
[42]P. Schwerdtfeger, ChemPhysChem **12**, 3143 (2011).
[43]M. Dolg and X. Cao, Chem. Rev. **112**, 403 (2012).
[44]A. N. Artemyev, "Effective QED Hamiltonians," in *Handbook of Relativistic Quantum Chemistry*, edited by W. Liu (Springer, Berlin, Heidelberg, 2016), pp. 1–19.
[45]E. J. Baerends, W. H. E. Schwarz, P. Schwerdtfeger, and J. G. Snijders, J. Phys. B: At., Mol. Opt. Phys. **23**, 3225–3240 (1990).
[46]V. Kellö and A. J. Sadlej, Int. J. Quantum Chem. **68**, 159 (1998).
[47]K. G. Dyall, Int. J. Quantum Chem. **78**, 412–421 (2000).
[48]T. Saue, R. Bast, A. S. P. Gomes, H. J. Aa Jensen, L. Visscher, I. A. Aucar, R. Di Remigio, K. G. Dyall, E. Eliav, E. Fasshauer *et al.*, J. Chem. Phys. **152**, 204104 (2020).
[49]T. Saue and T. Helgaker, J. Comput. Chem. **23**, 814 (2002).
[50]P. Pyykkö, Davidson Lecture, delivered for University of North Texas for 25 October 2013. Available at http://www.chem.helsinki.fi/~pyykko/Videos/UNT.mp4. AuCN is discussed at 47:44 of the video.
[51]A. L. Cyriaque Genet, F. Intravaia, and S. Reynaud, Ann. Fond. Louis Broglie **29**, 331 (2004), also available from the publisher's website: https://fondationlouisdebroglie.org/AFLB-Web/fldb-annales-index.htm.
[52]*Forces of the Quantum Vacuum: An Introduction to Casimir Physics*, edited by W. Simpson and U. Leonhardt (World Scientific, NJ, 2015).
[53]K. G. Dyall, C. W. Bauschlicher, D. W. Schwenke, and P. Pyykkö, Chem. Phys. Lett. **348**, 497 (2001).
[54]L. V. Skripnikov, J. Chem. Phys. **154**, 201101 (2021).
[55]L. V. Skripnikov, D. V. Chubukov, and V. M. Shakhova, J. Chem. Phys. **155**, 144103 (2021).
[56]A. Zaitsevskii, L. V. Skripnikov, N. S. Mosyagin, T. Isaev, R. Berger, A. A. Breier, and T. F. Giesen, J. Chem. Phys. **156**, 044306 (2022).
[57]J. A. Gaunt, Proc. R. Soc. London, Ser. A **122**, 513 (1929).
[58]M. Gell-Mann, Il Nuovo Cimento **4**, 848 (1956).
[59]S. S. Schweber, *An Introduction to Relativistic Quantum Field Theory* (Row, Peterson and Company, Evanston, IL, 1961).
[60]M. Peskin and D. Schroeder, *An Introduction to Quantum Field Theory*, Frontiers in Physics (Westview Press, 1995).
[61]W. Greiner and J. Reinhardt, *Field Quantization* (Springer-Verlag, Berlin, Heidelberg, 1996).
[62]G. C. Wick, Phys. Rev. **80**, 268 (1950).
[63]D. Kaiser, Am. Sci. **93**, 156 (2005).
[64]P. A. M. Dirac, Proc. R. Soc. London, Ser. A **136**, 453 (1932).
[65]W. H. Furry, Phys. Rev. **81**, 115 (1951).
[66]L. W. Fullerton and G. A. Rinker, Phys. Rev. A **13**, 1283 (1976).
[67]S. Klarsfeld, Phys. Lett. B **66**, 86 (1977).
[68]A. M. Frolov and D. M. Wardlaw, Eur. Phys. J. B **85**, 348 (2012).
[69]T. Beier, P. J. Mohr, H. Persson, and G. Soff, Phys. Rev. A **58**, 954 (1998).
[70]E. H. Wichmann and N. M. Kroll, Phys. Rev. **101**, 843 (1956).
[71]G. Källén and A. Sabry, Selsk., Mat.-Fys. Medd. **29**, 1 (1955).
[72]M. Baranger, H. A. Bethe, and R. P. Feynman, Phys. Rev. **92**, 482 (1953).
[73]I. Lindgren, *Relativistic Many-Body Theory: A New Field-Theoretical Approach*, 2nd ed. (Springer, 2016), Vol. 63.
[74]J. Malenfant, Phys. Rev. D **35**, 1525 (1987).
[75]P. Indelicato and P. J. Mohr, Phys. Rev. A **58**, 165 (1998).
[76]The $-\delta$ in Table 1 of Ref. 24 corresponds to $100 \times SE_{Li}/\Delta E_{Li}^{Hfs}$ with values taken from Table 2 of Ref. 77, where SE_{Li} in turn comes from S. A. Blundell, K. T.Cheng, and J.Sapirstein, Phys. Rev. A **55**, 1857 (1997).
[77]S. Boucard and P. Indelicato, Eur. Phys. J. D **8**, 59 (2000).
[78]F. Mandl and G. Shaw, *Quantum Field Theory* (John Wiley & Sons, 2010).
[79]V. B. Berestetskii, E. M. Lifshitz, and L. P. Pitaevskii, *Quantum Electrodynamics*, Course of Theoretical Physics Vol. 4 (Pergamon Press, Oxford, 1982).
[80]R. Hofstadter, Rev. Mod. Phys. **28**, 214 (1956).
[81]C. B. Lang and N. Pucker, *Mathematische Methoden in der Physik* (Spektrum Akademischer Verlag, 2016).
[82]R. J. Eden, Proc. R. Soc. London, Ser. A **210**, 388 (1952).
[83]R. Barbieri, J. A. Mignaco, and E. Remiddi, Il Nuovo Cimento A **11**, 865 (1972).
[84]J. Ginges and J. Berengut, Phys. Rev. A **93**, 052509 (2016).
[85]W. Greiner and J. Reinhardt, *Quantum Electrodynamics*, 4th ed. (Springer-Verlag, Berlin, Heidelberg, 2009).
[86]C. Itzykson and J.-B. Zuber, *Quantum Field Theory (Dover Books on Physics)* (Dover Publications, 1980).
[87]P. J. Mohr, Phys. Rev. A **46**, 4421 (1992).
[88]P. J. Mohr and Y.-K. Kim, Phys. Rev. A **45**, 2727 (1992).
[89]C. Thierfelder and P. Schwerdtfeger, Phys. Rev. A **82**, 062503 (2010).
[90]O. Fossgaard, O. Gropen, E. Eliav, and T. Saue, J. Comput. Phys. **119**, 9355 (2003).
[91]S. Dubillard, J.-B. Rota, T. Saue, and K. Faegri, J. Chem. Phys. **124**, 154307 (2006).
[92]K. G. Dyall, J. Chem. Phys. **139**, 021103 (2013).
[93]B. J. McKenzie, I. P. Grant, and P. H. Norrington, Comput. Phys. Commun. **21**, 233 (1980).
[94]C. Thierfelder, private communication (2022).
[95]A. D. Becke, J. Chem. Phys. **88**, 2547 (1988).
[96]V. I. Lebedev and D. N. Laikov, Dokl. Math. **59**, 477–481 (1999). Angular quadrature parameters available from http://server.ccl.net/cca/software/SOURCES/FORTRAN/Lebedev-Laikov-Grids/index.shtml.
[97]R. Lindh, P.-Å. Malmqvist, and L. Gagliardi, Theor. Chem. Acc. **106**, 178 (2001).
[98]DIRAC, a relativistic *ab initio* electronic structure program, release DIRAC22 (2022), written by H. J. Aa. Jensen, R. Bast, A. S. P. Gomes, T. Saue, and L. Visscher, with contributions from I. A. Aucar, V. Bakken, C. Chibueze, J. Creutzberg, K. G. Dyall, S. Dubillard, U. Ekström, E. Eliav, T. Enevoldsen, E. Faßhauer, T. Fleig, O. Fossgaard, L. Halbert, E. D. Hedegård, T. Helgaker, B. Helmich–Paris, J. Henriksson, M. van Horn, M. Iliaš, Ch. R. Jacob, S. Knecht, S. Komorovský, O. Kullie, J. K. Lærdahl, C. V. Larsen, Y. S. Lee, N. H. List, H. S. Nataraj, M. K. Nayak, P. Norman, G. Olejniczak, J. Olsen, J. M. H. Olsen, A. Papadopoulos, Y. C. Park, J. K. Pedersen, M. Pernpointner, J. V. Pototschnig, R. di Remigio, M. Repisky, K. Ruud, P. Sałek, B. Schimmelpfennig, B. Senjean, A. Shee, J. Sikkema, A. Sunaga, A. J. Thorvaldsen, J. Thyssen, J. van Stralen, M. L. Vidal, S. Villaume, O. Visser, T. Winther, S. Yamamoto, and X. Yuan, available at http://dx.doi.org/10.5281/zenodo.601045098, see also http://www.diracprogram.org.
[99]A. Sunaga, M. Salman, and T. Saue (2022). "4-component relativistic Hamiltonian with effective QED Potentials for molecular calculations: Dataset," Zenodo. https://doi.org/10.5281/zenodo.6874728
[100]L. Visscher and K. G. Dyall, At. Data Nucl. Data Tables **67**, 207 (1997).
[101]J. Sikkema, L. Visscher, T. Saue, and M. Iliaš, J. Chem. Phys. **131**, 124116 (2009).
[102]J. Pipek and P. G. Mezey, J. Chem. Phys. **90**, 4916 (1989).
[103]G. Knizia, J. Chem. Theory Comput. **9**, 4834 (2013).
[104]K. G. Dyall, J. Phys. Chem. A **113**, 12638 (2009).

[105]K. G. Dyall, Theor. Chem. Acc. **117**, 483 (2007).
[106]K. G. Dyall, Theor. Chem. Acc. **112**, 403–409 (2004).
[107]K. G. Dyall and A. S. P. Gomes, Theor. Chem. Acc. **125**, 97–100 (2010).
[108]K. G. Dyall, Theor. Chem. Acc. **129**, 603–613 (2011).
[109]K. G. Dyall, Theor. Chem. Acc. **135**, 128 (2016).
[110]K. G. Dyall, private communication (2021).
[111]K. G. Dyall, Theor. Chem. Acc. **108**, 335–340 (2002).
[112]K. G. Dyall, Theor. Chem. Acc. **115**, 441–447 (2006).
[113]K. G. Dyall, Theor. Chem. Acc. **131**, 1217 (2012).
[114]L. Visscher, T. J. Lee, and K. G. Dyall, J. Chem. Phys. **105**, 8769–8776 (1996).
[115]S. F. Boys and F. Bernardi, Mol. Phys. **19**, 553 (1970).
[116]J. G. Hill, A. O. Mitrushchenkov, and K. A. Peterson, J. Chem. Phys. **138**, 134314 (2013).
[117]J. Senekowitsch, "Spektroskopische eigenschaften aus elektronischen wellenfunktionen," Ph.D. thesis, Universität Frankfurt, Germany, 1988, The SURFIT program is available upon request from K. Peterson (Washington State).
[118]K. G. Dyall, J. Chem. Phys. **100**, 2118 (1994).
[119]L. Visscher and T. Saue, J. Chem. Phys. **113**, 3996 (2000).
[120]P. J. Stephens, F. J. Devlin, C. F. Chabalowski, and M. J. Frisch, J. Phys. Chem. **98**, 11623 (1994).
[121]A. D. Becke, J. Chem. Phys. **98**, 1372 (1993).
[122]J.-M. Lévy-Leblond, Commun. Math. Phys. **6**, 286 (1967).
[123]W. R. Johnson and G. Soff, At. Data Nucl. Data Tables **33**, 405 (1985).
[124]J. Thyssen, "Development and applications of methods for correlated relativistic calculations of molecular properties," Ph.D. thesis, University of Southern Denmark, 2001.
[125]In these calculations, the DIRAC keyword OPENFACTOR was set to one, such that orbital eigenvalues satisfy Koopmans' theorem.
[126]V. A. Yerokhin and V. M. Shabaev, J. Phys. Chem. Ref. Data **44**, 033103 (2015).
[127]L. Labzowsky, I. Goidenko, M. Tokman, and P. Pyykkö, Phys. Rev. A **59**, 2707 (1999).
[128]P. Zaleski-Ejgierd, M. Patzschke, and P. Pyykkö, J. Chem. Phys. **128**, 224303 (2008).
[129]D. B. Grotjahn, M. A. Brewster, and L. M. Ziurys, J. Am. Chem. Soc. **124**, 5895 (2002).
[130]T. Okabayashi, E. Y. Okabayashi, F. Koto, T. Ishida, and M. Tanimoto, J. Am. Chem. Soc. **131**, 11712 (2009).
[131]D. Figgen, G. Rauhut, M. Dolg, and H. Stoll, Chem. Phys. **311**, 227 (2005).
[132]A. Halkier, T. Helgaker, P. Jørgensen, W. Klopper, H. Koch, J. Olsen, and A. K. Wilson, Chem. Phys. Lett. **286**, 243 (1998).
[133]W. Gordy and R. L. Cook, *Microwave Molecular Spectra* (John Wiley & Sons, NY, 1970).
[134]J. Demaison, J. E. Boggs, and A. G. Császár, *Equilibrium Molecular Structures: From Spectroscopy to Quantum Chemistry* (CRC Press, 2016).
[135]T. Okabayashi, private communication (2020).
[136]K. Peterson, private communication (2021).
[137]X. Wang, L. Andrews, and V. Charlottes, J. Am. Chem. Soc. **2561**, 6581 (2003).
[138]P. Schwerdtfeger and M. Seth, J. Nucl. Radiochem. Sci. **3**, 133 (2002).
[139]A. Sunaga and T. Saue, Mol. Phys. **119**, e1974592 (2021).
[140]P. A. M. Dirac, Proc. R. Soc. London, Ser. A **126**, 360 (1930).
[141]P. A. M. Dirac, Proc. R. Soc. London, Ser. A **133**, 60 (1931).
[142]W. H. Furry and J. R. Oppenheimer, Phys. Rev. **45**, 245 (1934).
[143]C. D. Anderson, Phys. Rev. **43**, 491 (1933).
[144]S. Schweber, *QED and the Men Who Made It: Dyson, Feynman, Schwinger, and Tomonaga*, Princeton Series in Physics (Princeton University Press, 1994).
[145]W. Pauli and V. Weisskopf, "On the quantization of the scalar relativistic wave equation," in *Pauli and the Spin-Statistics Theorem*, edited by I. Duck and E. Sudarshan (World Scientific, 1998), pp. 238–255, excerpt from: Helv. Phys. Acta **7**, 709 (1934).
[146]A. Miller, *Early Quantum Electrodynamics: A Source Book* (Cambridge University Press, 1994).
[147]E. Majorana, "A symmetric theory of electrons and positrons (1937)," in *Ettore Majorana, Scientific Papers: On Occasion of the Centenary of His Birth*, edited by G.-F. Bassani and Council of the Italian Physical Society (Springer, Berlin, Heidelberg, 2006), pp. 218–231.
[148]S. Weinberg, *The Quantum Theory of Fields* (Cambridge University Press, 1995), Vol. 1.
[149]S. Weinberg, Daedalus **106**, 17 (1977), available at https://www.jstor.org/stable/20024506.
[150]J. Mehra, "Relativistic electrons and quantum fields," in *The Golden Age of Theoretical Physics* (World Scientific, 2001), Vol. 2, pp. 1030–1091.
[151]H. Kragh, *Dirac: A Scientific Biography* (Cambridge University Press, 1990).
[152]V. F. Weisskopf, Phys. Today **34**(11), 69 (1981).
[153]T. Ohlsson, *Relativistic Quantum Physics: From Advanced Quantum Mechanics to Introductory Quantum Field Theory* (Cambridge University Press, 2011).
[154]M. Gell-Mann and F. Low, Phys. Rev. **84**, 350 (1951).
[155]A. Fetter and J. Walecka, *Quantum Theory of Many-Particle Systems (Dover Books on Physics)* (Dover Publications, 2012).
[156]J. Sucher, Phys. Rev. **107**, 1448 (1957).
[157]F. J. Dyson, Phys. Rev. **75**, 1736 (1949).
[158]L. N. Labzowsky, G. L. Klimchitskaya, and Y. Dmitriev, *Relativistic Effects in the Spectra of Atomic Systems* (Institute of Physics Publishing, Bristol; Philadelphia, 1993).
[159]F. J. Dyson, Phys. Rev. **75**, 486 (1949).
[160]J. Schwinger, Phys. Rev. **74**, 1439 (1948).
[161]J. D. Bjorken and S. D. Drell, *Relativistic Quantum Fields* (McGraw-Hill, 1965).
[162]P. J. Mohr, G. Plunien, and G. Soff, Phys. Rep. **293**, 227 (1998).
[163]M. D. Schwartz, *Quantum Field Theory and the Standard Model* (Cambridge University Press, Cambridge, 2014).
[164]R. P. Feynman, Phys. Rev. **76**, 749 (1949).
[165]P. J. Mohr, AIP Conf. Proc. **189**, 47 (1989).
[166]P. J. Mohr, Phys. Rev. A **32**, 1949 (1985).
[167]I. Lindgren, "Many-body problems in atomic physics," in *Recent Progress in Many-Body Theories: Volume 3*, edited by T. L. Ainsworth, C. E. Campbell, B. E. Clements, and E. Krotscheck (Springer, Boston, MA, 1992), pp. 245–276.
[168]P. Indelicato and P. J. Mohr, Phys. Rev. A **46**, 172 (1992).
[169]W. H. Furry, Phys. Rev. **51**, 125 (1937).
[170]W. Greiner, *Relativistic Quantum Mechanics*, 3rd ed. (Springer, Berlin, Heidelberg, 2000).
[171]M. Gyulassy, "Higher order vacuum polarization for finite radius nuclei: Application to muonic lead and heavy ion collisions," Ph.D. thesis, University of California, Berkeley, 1974.
[172]J. Blomqvist, Nucl. Phys. B **48**, 95 (1972).
[173]A. G. Fainshtein, N. L. Manakov, and A. A. Nekipelov, J. Phys. B: At., Mol. Opt. Phys. **24**, 559 (1991).
[174]H. A. Bethe, Phys. Rev. **72**, 339 (1947).
[175]P. J. Mohr, Ann. Phys. **88**, 26 (1974).
[176]N. J. Snyderman, Ann. Phys. **211**, 43 (1991).
[177]V. A. Yerokhin and V. M. Shabaev, Phys. Rev. A **60**, 800 (1999).
[178]W. Pauli and F. Villars, Rev. Mod. Phys. **21**, 434 (1949).
[179]G. 't Hooft and M. Veltman, Nucl. Phys. B **44**, 189 (1972).
[180]C. G. Bollini, J. J. Giambiagi, and A. G. Domínguez, Il Nuovo Cimento **31**, 550 (1964).
[181]E. Zeidler, *Quantum Field Theory II: Quantum Electrodynamics: A Bridge between Mathematicians and Physicists* (Springer, 2009), Vol. 2.
[182]J. C. Collins, *Renormalization: An Introduction to Renormalization, the Renormalization Group and the Operator-Product Expansion*, Cambridge Monographs on Mathematical Physics (Cambridge University Press, 1984).
[183]K. Huang, *Quantum Field Theory: From Operators to Path Integrals* (John Wiley & Sons, 2010).
[184]K. Huang, Int. J. Mod. Phys. A **28**, 1330050 (2013).